# Hudson Geotraverse: Geology of the Mid-Atlantic Ridge at 45 degrees N

F. Aumento, B. D. Loncarevic and D. I. Ross

| **Email alerting service** | Receive free email alerts when new articles cite this article - sign up in the box at the top right-hand corner of the article or click **here** |
|---|---|

# IV. REGIONAL STUDIES

## Hudson Geotraverse: geology of the Mid-Atlantic Ridge at 45° N

By F. Aumento†

*Department of Geology, Dalhousie University, Halifax, N.S., Canada*

B. D. Loncarevic and D. I. Ross

*Atlantic Oceanographic Laboratory, Bedford Institute, Dartmouth, Canada*

A strip across the Crest Mountains and High-Fractured Plateau of the Mid-Atlantic Ridge has been surveyed systematically between latitudes 45 and 46° N. Continuous bathymetric, magnetic and gravimetric data have been obtained. Seismic refraction experiments have revealed a complex structure lineated parallel to the axis of the Ridge. Seismic reflexion studies have revealed a picture of the sediment cover, and have shown the possible existence of block faulting of the underlying rocks, with faults alined both parallel and at right angles to the axis of the Ridge. The major rock types found in 46 dredge stations can be grouped as follows:

(1) Ubiquitous basalts and tuffs (ranging from theoleiites to alkali basalts, with a few ferro-basalts and high-Al basalts). Basalts rich in resorbed high-calcic plagioclase xenocrysts are common; these occur both on the slopes of shield volcanoes and in the deepest hole of the Median Valley. A nearby fault scarp yielded coarse-grained gabbros.

(2) Serpentinized mafic and ultramafic rocks are not restricted to elongated, presumably block-faulted seamounts, but are also common on the slopes of what had been interpreted on morphological grounds as shield volcanoes; they are absent, however, on the Median Valley floor and its immediate scarp slopes. The pre-serpentinization rock types include dunites, harzburgites, gabbros, troctolitic gabbros and amphibolitic peridotites showing crude cumulate textures.

(3) The lower parts of the steep inner walls of the Median Valley have yielded metabasalts and metadiabases showing alteration within the greenschist facies of metamorphism, whilst still retaining original igneous characteristics.

(4) Restricted to the fault scarps of elongated seamounts further removed from the Median Valley are higher grade metamorphic rocks of the almandine amphibolite facies of metamorphism. These rocks have lost all igneous textures and exhibit a strong gneissic fabric.

(5) Three localities yielded dioritic rocks in association with serpentinized ultramafics. The diorites vary in character from hornblende-rich quartz diorites to more siliceous, almost hornblende-free trondhjemites. The latter show considerable albitization. The whole suite of rocks shows great affinities with similar suites found as late stage intrusives in alpine-type ultramafic complexes.

About 23 % of the specimens collected included gneissic, granitic and sedimentary rock types of erratic origin, ice rafted into the area in the Pleistocene. A study of their distribution indicates that there are no erratics in the Median Valley, that they are scarce on the mountain ranges immediately flanking the Valley, but beyond these areas they are abundant and are randomly distributed over the whole area. Such a distribution may be a result of ocean-floor spreading, indicating that the Median Valley is younger than the last ice age, or that extrusions subsequent to the last ice age have engulfed any erratics present in the Median Valley.

The thickness of manganese coating on extrusive rocks and their K/Ar and fission track ages increase systematically with distance on either side of the axis of the M.A.R., strongly supporting the ocean-floor spreading hypothesis. The ages and coatings both show a marked change in their rate of increase beyond a distance of 50 to 60 km on either side of the axis. The position at which this occurs coincides with the thickening in these areas of sediments found in the inter-volcanic valleys, and the morphological changes between the Crest Mountains and the High-Fractured Plateau. The combined data strongly suggest that there was either a quiescent period sometime in the Pliocene during which ocean-floor spreading was inactive, or that the rate of spreading had accelerated during the Pliocene from less than 1 cm a⁻¹ to a computed 2.5 cm a⁻¹ in Pleistocene times.
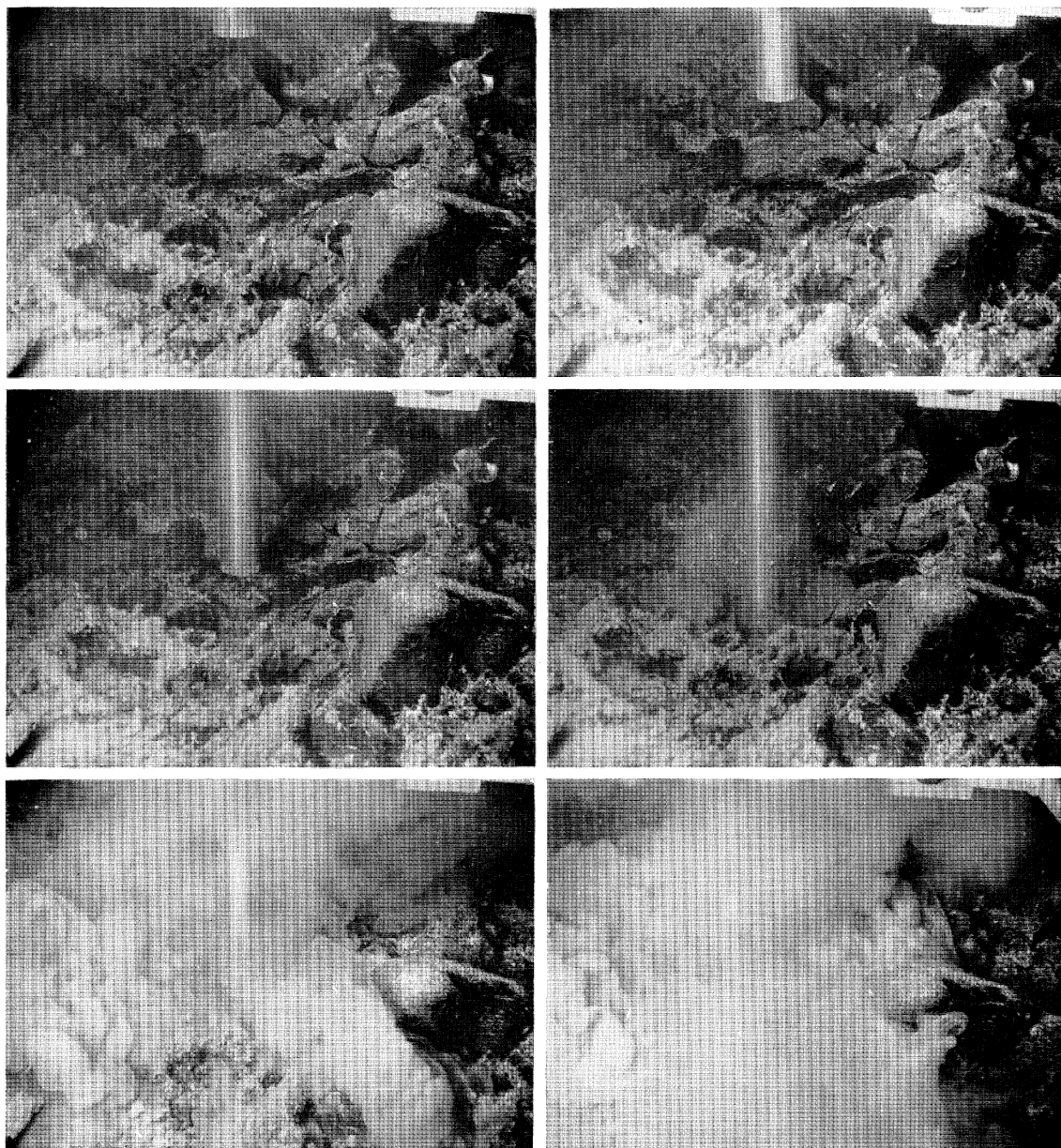
Drilling on the Mid-Atlantic Ridge in 1060 m (F. Aumento, Dalhousie).

Hudson Geotraverse is a cooperative project organized by the Atlantic Oceanographic Laboratory, Bedford Institute, Dartmouth, Canada, to study the geology and geophysics of a 1° wide strip of the Atlantic Ocean between the latitudes of 45 and 46° N and longitudes 18 to 60° W. The 380 000 km² area stretches from Cape Breton, N.S., across the Grand Banks of Newfoundland to the eastern flank of the Mid-Atlantic Ridge. This geotraverse crosses most of the major oceanic provinces recognized so far, except for a deep-sea trench.
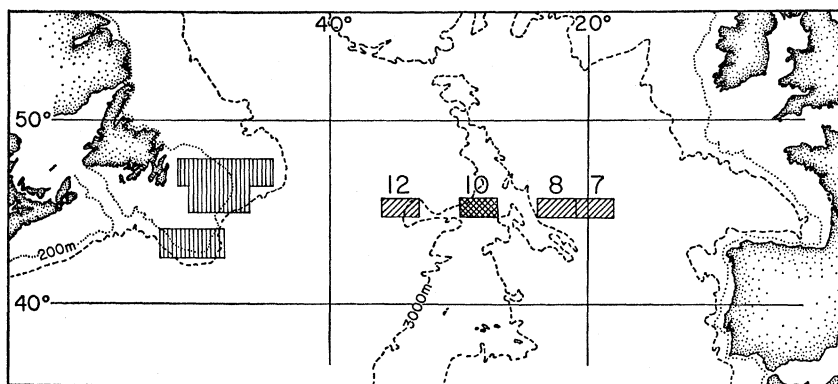


FIGURE 1. Index chart of the North Atlantic Ocean showing the location of the Hudson Geotraverse. Plotting sheets along the Geotraverse for which bathymetric, gravimetric and magnetic data are available are shaded: sheet 10 covers the area on the Crest of the M.A.R. which is discussed in this paper.

The first-stage exploration of the Hudson Geotraverse has involved six deep-sea and three continental shelf expeditions by three Canadian and one British research vessel (see figure 1). This paper is primarily concerned with the geology and geophysics of the Crest Mountains and western High Fractured Plateau of the Ridge at 45° N, and there will be no mention of other studies elsewhere along the geotraverse.

The data presented below will show that:

(a) Whereas ocean-floor spreading from a central axis can be demonstrated, the Ridge at 45° N lacks a well-defined axis of symmetry; this is evident from bathymetric, gravimetric, magnetic and chronological investigations.

(b) There is conflicting evidence both for and against major variations in the spreading rates during the last 16 Ma.

(c) Except for the high positive magnetic anomaly over the Median Rift Valley and a second positive anomaly on the western High Fractured Plateau, intermediate anomalies are highly confused and difficult to interpret directly. Palaeomagnetic, petrological and seismic data suggest that the anomalies are produced primarily from rocks forming the upper parts of oceanic layer 2.

(d) There is anisotropy in the seismic mantle velocity of layer 4.

(e) There is a continuous series from quartz-normative tholeiites through to nepheline-normative alkali basalts on the ocean floor, with minor amounts of ferro-basalts and high-alumina basalts, the latter two showing affinities to both tholeiites and alkali basalts.

(f) Gravity crystal differentiation during quiescent conditions beneath the floor of the Median Rift Valley produces magmas for the extrusion of basalts and forms pseudostratiform gabbroic and ultramafic masses showing crude cumulate textures and mineral layering.

(g) Magmatic differentiation proceeds as far as to produce quartz-diorites and trondhjemite intrusions in the later stages of igneous activity.

(h) Metamorphism is superimposed onto the igneous stratigraphy of basalt–diabase–gabbro. The lower part of layer 2 may reach the highest greenschist facies conditions, and layer 3 those of the almandine amphibolite facies (minimum temperature/pressure conditions for the latter being 550 °C and 4000 bar $(0.4 \text{ GN m}^{-2})$ at depths of less than 7 km below sea level).

(i) Block faulting and upthrusting of layers 2 and 3 may be related to the diapiric intrusion of serpentinized peridotite through these layers. Serpentinization takes place both before and during emplacement under maximim temperature conditions (485 °C).

## The survey

Table 1 summarizes the extent of the surveys that have been conducted to date as part of the Hudson Geotraverse programme on the crest of the Mid-Atlantic Ridge.

The surveys on the flanks and crest of the M.A.R. are outside the range of precise radio navigation aids. Accurate relative positioning of survey ships was based on a network of moored radar transponder buoys (Loncarevic 1969).

### Table 1. Summary of surveys and station work on the Crest Mountains and High Fractured Plateau of the Mid-Atlantic Ridge at 45° N

| date | ship | survey/km. Bathymetry magnetics and gravity | successful stations | | | | | | |
|------|------|------|-------|--------|------|--------|-------|---------|----------------|
| | | | total | camera | core | dredge | drill | hydrog. | vert. plankt. |
| 1960 | *Discovery* | 430 | 5 | 3 | — | 2 | — | — | — |
| 1965 | *Hudson* | 1950 | — | — | — | — | — | — | — |
| 1966 | *Hudson* | 6950 | 62 | 17 | 11 | 9 | 2 | — | 23 |
| 1968 | *Hudson* | 13940 | 87 | 8 | 8 | 26 | — | 18 | 27 |
| 1968 | *Theta* | — | 3 | — | — | 3 | — | — | — |
| 1969 | *Hudson* | — | 28 | — | 4 | — | 12 | — | 12 |

Fifty-three radar transponder buoys were used to control the survey of 29 000 km² of the Crest Mountains and western High Fractured Plateau of the M.A.R. (area 10, figures 1 and 2). During the 1960, 1965 and 1966 surveys there were no means of accurately positioning the buoys. By the simultaneous use of a number of buoys it was possible to survey the area without absolute reference to the surface of the Earth. However, the errors inherent in fixing the buoys relative to each other are cumulative and, as the coverage increases, become unacceptable. During the 1968 expedition satellite navigation was used to establish the positions of the buoys and to monitor their surface movement. Accurate composite charts were compiled by overlapping data from the various surveys. The ship's tracks over the entire crestal area for which continuous bathymetric, magnetic and gravimetric data are available are shown in figure 2.

## Bathymetry

The most conspicuous feature of the area (see figure 3) is the Median Rift Valley, a linear feature trending to 019°, arbitrarily delineated by the 2560 m (1400 fathoms) contour (Loncarevic, Mason & Matthews 1966). The mean width of the valley, taken as the distance between these contours on opposite walls, is 9.5 km. However, at the southern and northern extremities of the region the valley narrows considerably, where it is blocked by the outpourings from pairs

of flank volcanoes (Muir & Tilley 1964; Loncarevic *et al.* 1966). In the north-central region, at 45° 40′ N, the valley broadens to 18.6 km, but narrows rather abruptly immediately north-wards. The westernmost part of the widest section of the valley is bounded by a steep cliff running east–west for about 6 km. This may be the surficial expression of a small transverse fault.
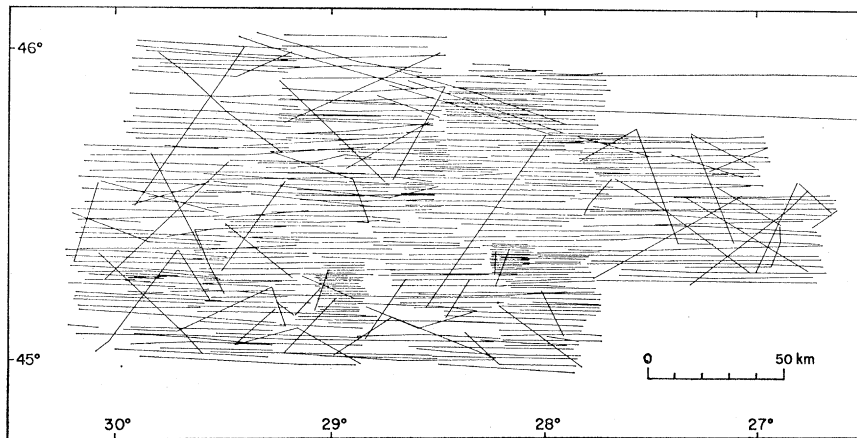


FIGURE 2. C.S.S. *Hudson* track chart for area 10 of figure 1 on the Crest and High Fractured Plateau of the M.A.R. for which complete bathymetric, gravimetric and magnetic data are available. The tracks were controlled by 53 moored radar transponder buoys and 270 satellite navigation fixes.

The floor of the valley cradles five basins, with depths exceeding 2900 m, separated by small ridges and rises. In general the depressions become deeper northwards, so that the greatest depth (3520 m) is found at 45° 41.4′ N, 27° 47.7′ W. There is no correlation between the depth and the width. The valley floor is almost completely devoid of sediments, and several attempts to recover a sediment core failed. Bottom photographs confirm these observations (Aumento 1968).

To the west of the Median Valley are the Crest Mountains, a 52 km wide region of rough, linear topography with considerable relief. They have a mean depth of about 2360 m, though five basins exceed 2560 m. The latter have only a thin veneer of sediments. However, ponded sediments have been found in isolated valleys, with thicknesses of up to 300 m (Keen & Manchester 1969). The seamounts in the south of this region are generally larger and more distinct than those in the north. The Crest Mountains are bounded to the west by the 2560 m contour, a distinct physiographic boundary separating the former from the High Fractured Plateau region to the west.

To the west of this boundary the sediment thickness increases considerably and substantial areas are under flat lying sediments (Keen & Manchester 1969). The average depth increases to about 2900 m, deepening gradually westward; at the western limits of the survey, depths equal to those at the bottom of the Median Valley are encountered again. Within this west High Fractured Plateau region the seamounts are distinct, isolated features, especially in the south.

Due to insufficient coverage of the eastern Crest Mountains, topographic symmetry (with respect to the axis) cannot be evaluated. In the western region the nearest basin to the Median Valley with a depth exceeding 2700 m is 54 km west of it, whereas similar depths are encountered at only half that distance to the east. Even more surprising is that the second highest peak of the survey area, Mount Kettle, is found on the eastern flank of the crestal region, away from the high crests overlooking the Median Valley. The accentuated topography of the eastern Crest Mountains suggests that the eastern region is more fractured than the western region.
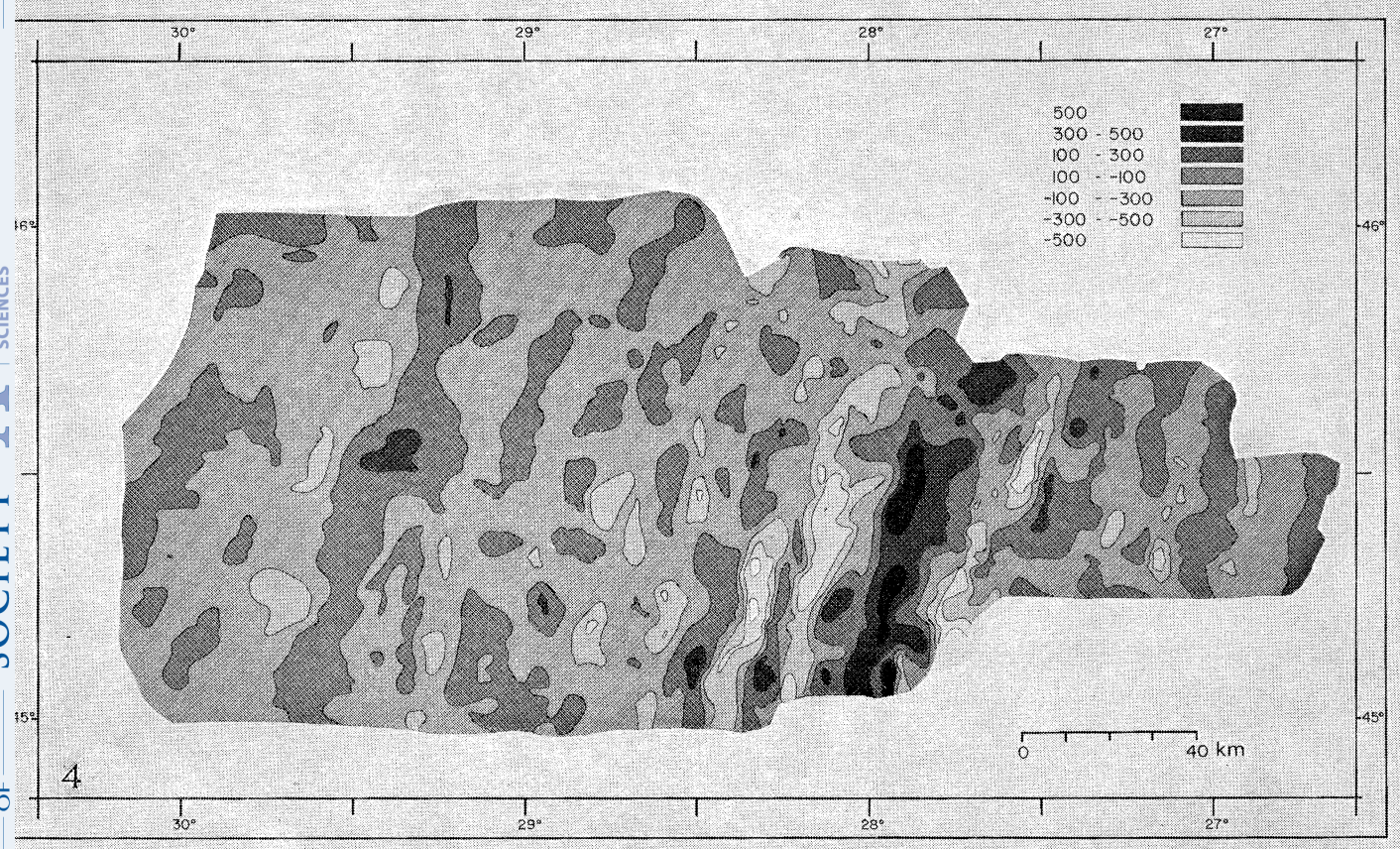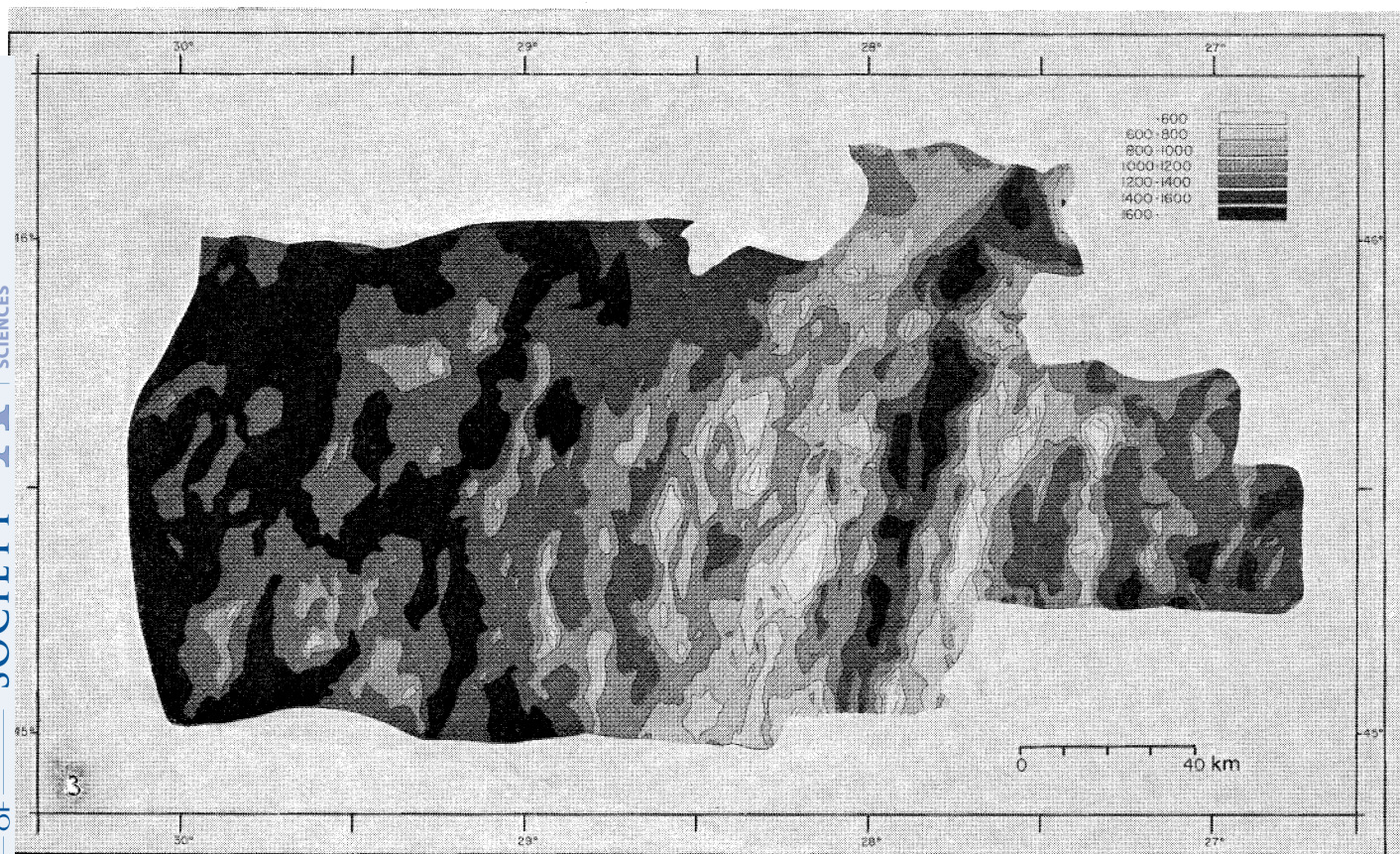
FIGURE 3. Bathymetry of the Crest Monutains and western High Fractured Plateau of the M.A.R. at 45° N, contoured at 200 fathoms (365.6 m) intervals uncorrected for the speed of sound in water. The Median Rift Valley lies between 27° 30′ W, 46° N and 28° W, 45° N.

FIGURE 4. Magnetic anomalies over the crest Mountains and western High Fractured Plateau of the M.A.R. at 45° N, calculated by subtracting a third degree polynomial from the observations recorded at two minute intervals along the ship's tracks.

## MAGNETICS

The magnetic anomaly pattern (see figure 4) is dominated by a strong positive lineation, coincident in position with the Median Valley. Within this central anomaly are two higher peaks, associated with the two southern depressions in the valley floor (500 $\gamma$† near 45° 17′ N, over 800 $\gamma$ near 45° 27′ N). The individual anomalies are not symmetrical but are shifted to the west, with gradients towards the west steeper than those towards the east.

To the east and west, the central positive anomaly is flanked by elongated negative anomalies everywhere less than $-200\,\gamma$ (as far as 45° 40′ N). Within these negative bands there are large negative peaks of greater amplitude. These peaks are in line with the two positive peaks contained within the central anomaly band; this suggests that the amplitudes of the negative anomalies are correlated with those of the positive anomalies.

Farther to the west the anomaly pattern is very confusing. However, a pattern of elongated anomalies parallel to the central anomaly is discernible in figure 4. The continuity (length) of these anomalies is variable until at 45° N, 29° 40′ W a continuous positive band with a maximum amplitude of $+350\,\gamma$ is found crossing the whole survey area. In comparison with the Reykjanes Ridge, other surveys and model calculations, this band corresponds to anomaly 5, for which Pitman, Herron & Heirtzler (1968) give the age 8.79 to 9.94 Ma before present. If the identification of this anomaly is correct, then a mean rate of spreading for the last 10 Ma can be calculated to be around 1.28 a⁻¹.

The contrast between the continuity of anomaly 5 and the randomness of the pattern during the period 2 to 8 Ma ago is very significant. Randomness of dyke injection (Matthews & Bath 1967) at the crest alone could not account for such widespread disruption of the pattern. Instead we suggest that due to changes in the velocity and direction of spreading, compressional forces were generated in the tectonic plate underlying the region and that these forces affected the magnetic pattern by: fracturing, block faulting and gravitational sliding, which would mix up material with different directions of magnetization; changing the character and nature of magnetic remanence of the crustal rocks by metamorphism; forcing new lavas to erupt through fissures at different times; and assisting the diapiric intrusion of highly magnetic serpentinized ultramafic rocks, such that their magnetization would be unrelated to the basic pattern of a spreading ocean floor.

## GRAVITY

The free-air gravity anomaly chart for the crestal region is shown in figure 5. Comparison with the bathymetry of figure 3 indicates that the free air anomalies reproduce the morphological trends.

The entire area is a region of free air gravity anomaly with a 'normal' value ranging from 30 mgal‡ on the western edge of the area and increasing to approximately 70 mgal at the crest. The Median Valley is marked by a low linear anomaly between 50 and 30 mgal. In the southern half of the area the pair of block-faulted seamounts on either side of the Median Valley (Confederation Peak and Mount Olympus) produce well defined positive anomalies in excess of 130 mgal, whereas at the northern end, Gog and Magog Mountains, which are thought to be volcanoes, produce little gravitational effect.

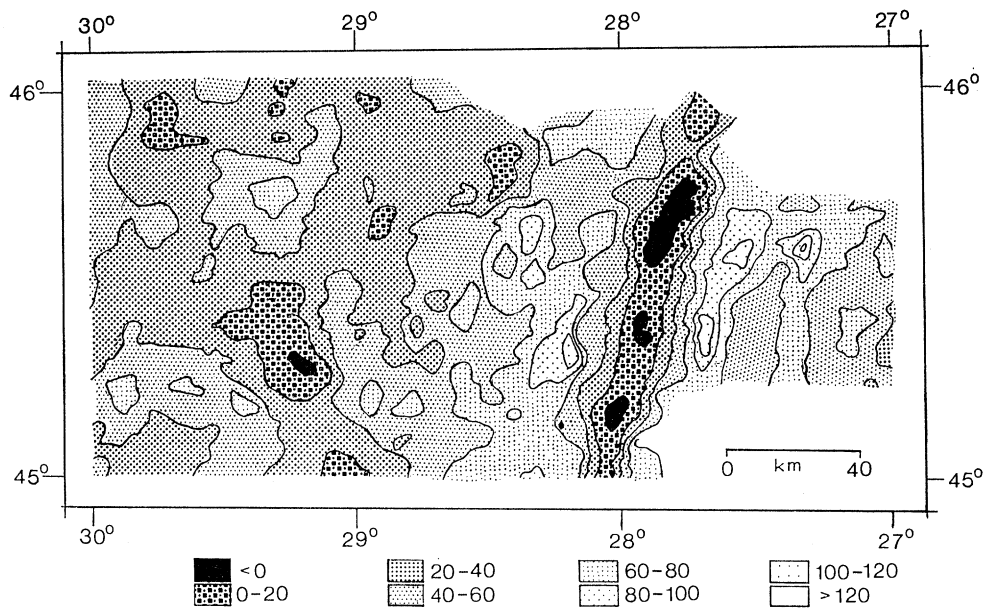† $1\,\gamma = 1\,\mathrm{nT}$; ‡ $1\,\mathrm{gal} = 1\,\mathrm{cm\,s^{-2}}$.

FIGURE 5. Free air gravity anomaly chart for the Crest Mountains and western High Fractured Plateau of the M.A.R. at 45° N.

## SEISMICS

Two detailed seismic refraction experiments were carried out on the crestal region (Keen & Tramontini 1969). M.V. *Theta* acted as shooting ship while C.S.S. *Hudson* was the receiving ship. Telemetering moored sonobuoys were used as detectors in conjunction with a seismic cable floated astern of *Hudson*. The position of the receivers, located by satellite navigation fixes, and the locations of the two experiments with respect to the Median Valley, are shown in figure 6.

A total of 348 shots were fired in the two experiments. Using multiple receivers with good areal distribution enabled the time–term method of interpretation to be used.

Three dominant seismic layers were detected, namely the oceanic layers 2, 3 and 4 of the ocean basins, with velocities ranging from 3.5 to 5.4 km s$^{-1}$ for layer 2, 5.8 to 6.8 km s$^{-1}$ for layer 3, and 8.1 km s$^{-1}$ for layer 4 beneath the Mohorovičić discontinuity.

Layers 2 and 3 may not be continuous over the area, since one or both may be absent on many of the time–distance plots. The mean thickness of layer 3 (3.4 km) may be less near the axis of the Ridge (1.3 km), while layer 2 (mean thickness 1.6 km) may be somewhat thicker (up to 2 km). In addition, layer 2 may be subdivided into two discontinuous layers with velocities of 3.8 and 4.7 km s$^{-1}$ for the upper and lower layers respectively. Additional, discontinuous thin reflectors, with velocities of 2.2 and 2.8 km s$^{-1}$, overlie layer 2 on the High Fractured Plateau, but are completely absent on the Median Rift Valley. In the latter locality a single reflector with velocity 3.3 km s$^{-1}$ overlies a single layer 2 of velocity 4.7 km s$^{-1}$.

The mean depth to the Moho is 7.5 km, but there exist depth variations of up to 3 km over the area. Layer 4, the Upper Mantle, has a mean velocity of 8.1 km s$^{-1}$, with an anisotropy of ± 0.25 km s$^{-1}$, the azimuth of maximum velocity being at 080°, a direction which is not perpendicular to the 019° strike of the axis of the Ridge. No evidence was found for anomalous

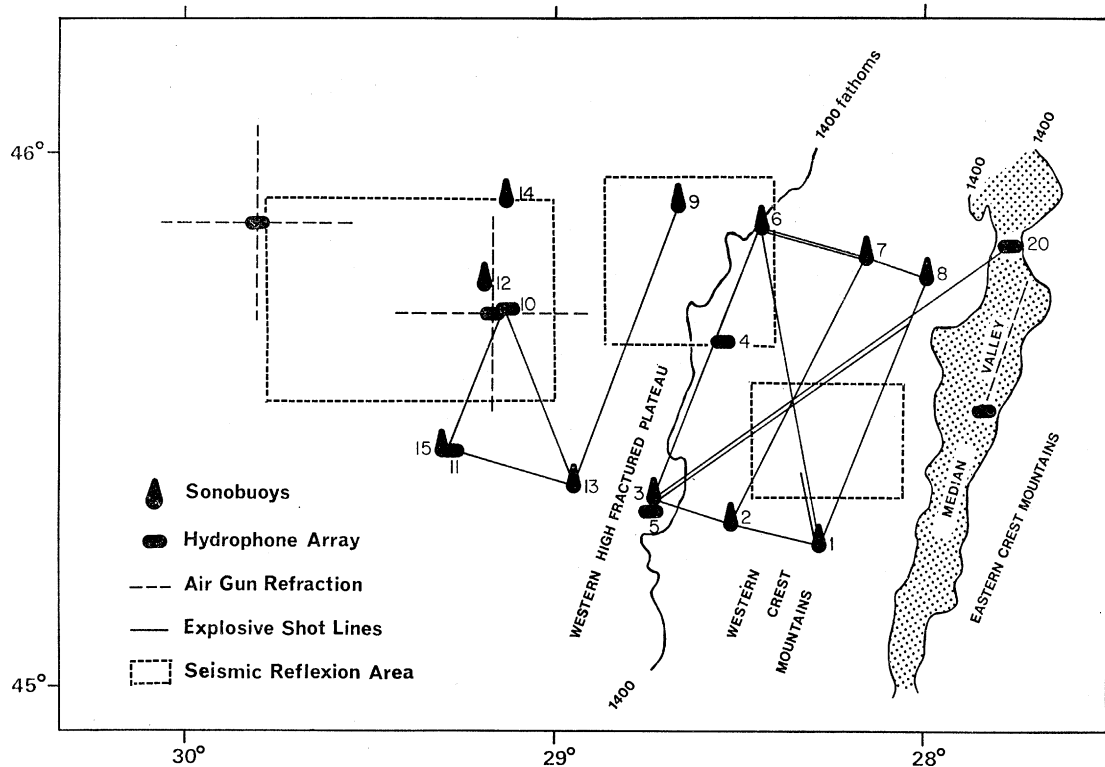mantle material, except beneath the Median Valley, where mantle velocities of 7.5 km s$^{-1}$ were measured.



FIGURE 6. Location of three sets of seismic experiments carried out at 45° N: (1) two refraction experiments using moored sonobuoy receivers, (2) three air-gun (2000 in³; 33 dm³) refraction experiments using a towed hydrophone array (3) three air-gun (10 in³; 165 cm³) reflexion surveys of sediment attitudes and thicknesses.

In addition to the refraction experiments, seismic reflexion studies were carried out using a 10 in³ (165 cm³) airgun as sound source. A gross picture of the sediment cover on the Crest and High Fractured Plateau was obtained out to about 130 km west of the Median Valley. Details of the sediment cover were also obtained in a valley just west of the Median Valley and in an area towards the western edge of the survey area (figure 6). In the valleys near the axis the sediment is relatively undeformed, and in terms of two-way travel times is up to 250 ms thick. The sediment cover is more general and thicker beyond about 60 km from the axis. The pattern of coverage on peaks on the High Fractured Plateau is indicative of block faulting, the faults being alined both parallel and at right angles to the axis of the Ridge.

Seismic velocities measured at sea were correlated with seismic velocities measured in the laboratory on specimens dredged from the area, as follows:

| velocity | rock type |
| --- | --- |
| 2.2 | foraminiferal sand and ooze |
| 2.8 | highly weathered material and compacted sediment |
| 3.8 | weathered pillow basalt and weathered serpentinite |
| 4.7 | massive basalt, diabase and fresh serpentinite |
| 5.8–6.8 | meta-basalts, gabbros and meta-gabbros |

### Bottom sampling

The survey area across the Crest Mountains and High Fractured Plateaus was sampled successfully at 46 dredge stations, 23 piston-core stations, 14 rock-core drill stations, 10 hydrographic stations (Garner & Ford 1969), 26 camera stations, and 62 vertical plankton stations. The positions of these stations (except for the vertical plankton stations, which were collected for foraminiferal studies and are too numerous for effective plotting on the scale available) are shown in figure 7 and the relative yields of the dredge stations are shown schematically in figure 8. Additional hard-rock specimens were obtained with the rock-core drill; the latter yielded eleven oriented cores of lithified foraminiferal and coralline material, two oriented cores of fresh basalt, and one core consisting of a combination of the two lithologies.
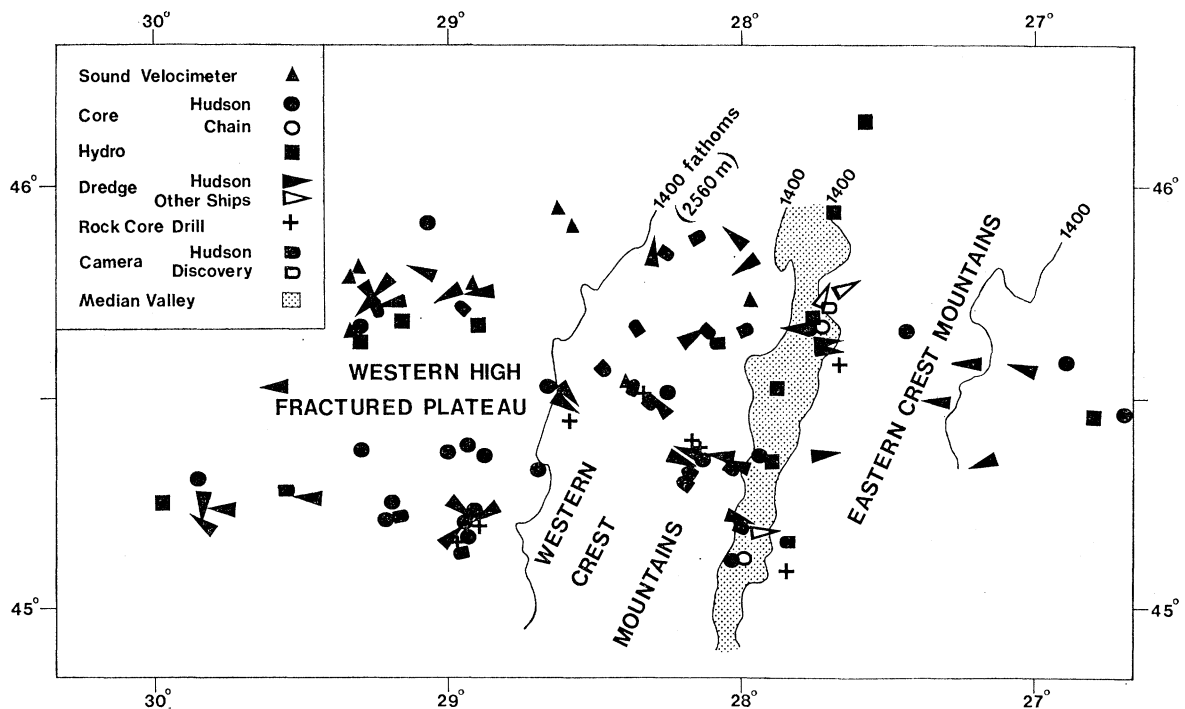


FIGURE 7. Sampling stations on the Crest and High Fractured Plateau of the M.A.R. at 45° N undertaken from C.S.S. *Hudson*, M.V. *Theta*, R.S.S. *Discovery* and R.V. *Chain* during the last 9 years.

Most of the Hudson stations were taken within range or one or more of the moored radar transponder buoys; satellite fixes were also used during station keeping whenever possible. In addition, to determine the exact positions of the dredges on the sea floor, the ship to dredge range was telemetered by a precision timed pinger mounted on the cable 20 m above the dredge synchronized with the ship's precision depth recorders. A bathykymograph placed immediately in front of the dredge recorded time, depth and periods of major abrasions with the ocean floor. The combined information retrieved from the transponders, the pinger, the bathykymograph and the load cell monitoring the load on the cable pulling the dredge permitted a good estimate to be made of the location and depth at which samples were collected (Aumento 1970).

Yields from the 1960 *Discovery* and 1966 *Hudson* expeditions (total of 10 dredge stations) have already been described in detail (Muir & Tilley 1964, Aumento 1968, Aumento & Loncarevic
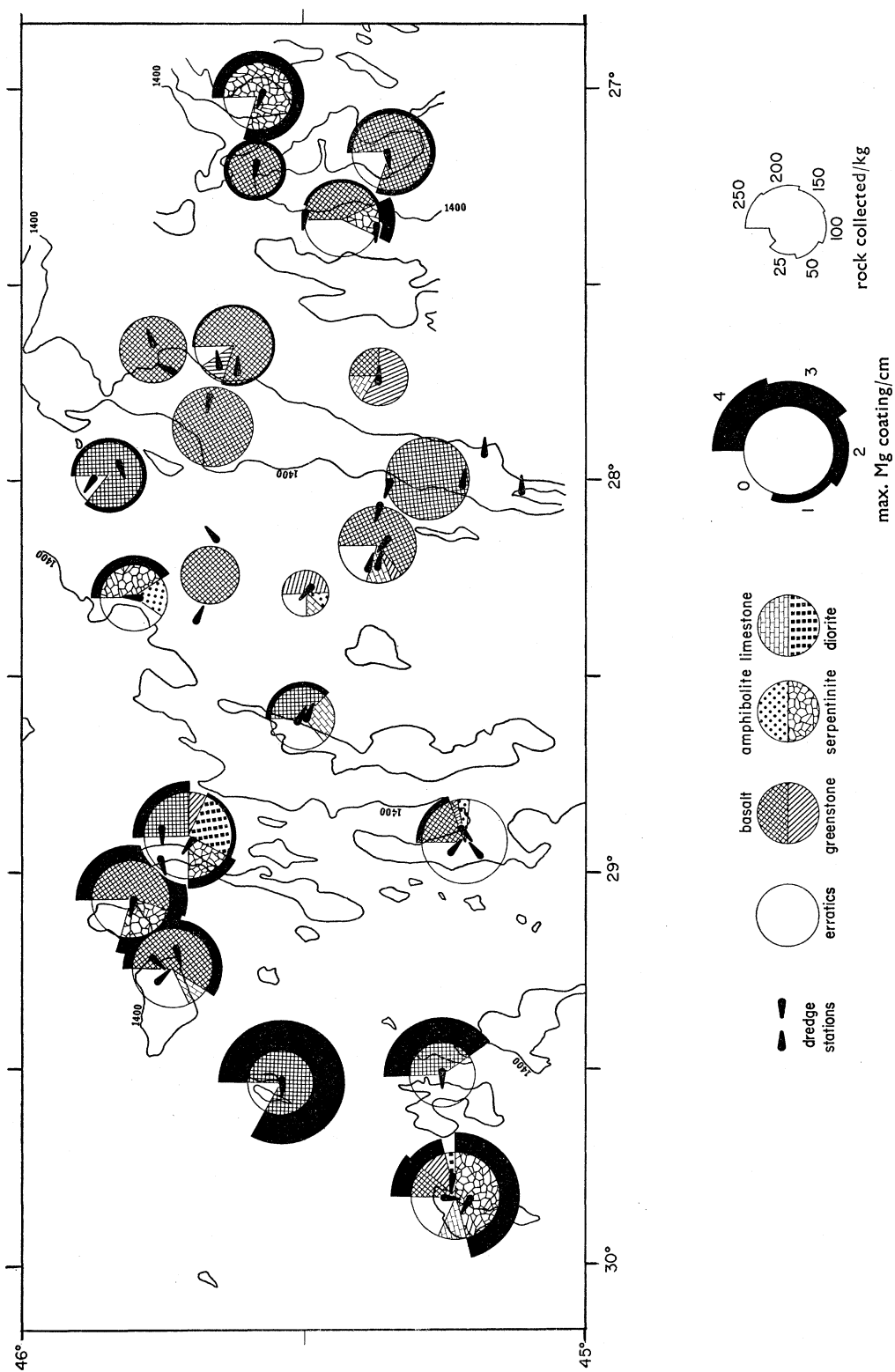
FIGURE 8. Distribution of the dredge stations about the axis of the M.A.R. at 45° N, showing the rock types collected, the maximum accumulation of ferro-manganese coating (centimetres), the total mass of rocks (kg) collected at each station (after Aumento 1969b). Contours in fathoms.

1969) as have fission track and preliminary K–Ar dates (Fleischer, Viertl, Price & Aumento 1968; Aumento, Wanless & Stevens 1968; Aumento 1969*b*). The additional 28 stations undertaken in the summer of 1968 have complicated the geological picture considerably. Although basalts (mainly tholeiites, with a few alkali basalts, ferro-basalts and spilites) still account for most of the rocks exposed in the area, serpentinized mafic and ultramafic rocks have also become of major importance, and the presence of greenstones and amphibolites has also been established. In addition, dioritic rocks of intermediate to acid character were recovered at three localities (Aumento 1969*a*).

### Basalts, diabases and gabbros

Textures encountered for the basic rocks vary from the glassy, sometimes spherulitic pillow lavas common to the Median Valley and most other sampling locations, to more massive, diabasic and gabbroic textures restricted to fault scarps. The pillow basalts are often vesicular; vesicle size shows no correlation whatsoever with depth of extrusion. Many of the glassy basalts are rich in resorbed calcic plagioclase xenocrysts. These were interpreted as derived from concentration of these crystals in cupolas beneath the volcanoes: on subsequent extrusion the crystals resorbed due to a temporary superheating of the magmas caused by sudden pressure releases (Muir & Tilley 1964; Aumento 1968). However, in 1968 these xenocryst-rich basalts were also found at the very bottom of the deepest hole of the Median Valley, suggesting that cupolas of magma may exist beneath the Valley floor. These magma chambers must be stagnant and undisturbed for considerable periods of time to allow gravity crystal differentiation to take place and hence produce the high concentrations of calcic plagioclase xenocrysts.

Near the base of a fault scarp close to the outcrop of these xenocryst-rich basalts in the Median Valley there occur coarse gabbros (of tholeiitic character) and diabases showing incipient metamorphism in the greenstone facies. These gabbros are overlain by coarse basalts and pillow lava, suggesting that such a fault scarp exposure represents a section through what had once been the sequence beneath the Median Valley: i.e. pillow lava extrusions fed by a cupola; the latter was able to crystallize more slowly than the basalts, giving rise to cumulate gabbroic textures.

The basalts show considerable chemical variations. Sixty complete basalt analyses are now available from the area at 45° N (a complete data file of analyses and other information is available as an unpublished report from the Atlantic Oceanographic Laboratory). These analyses have been plotted onto histogram-type distribution diagrams showing statistically the relative percentages of samples analysed expected to fall into particular compositional fields. Figure 9, which shows their distribution in the normative system diopside–hypersthene–olivine–quartz–nepheline, clearly indicates that there exists a continuous variation from quartz normative tholeiites to nepheline normative alkali basalts. However, a higher proportion of the basalts does fall into the low olivine normative field, and an additional, but less significant, peak falls in the area of incipient normative nepheline occurrence. An additional 'lobe' extending into the high-diopside quartz-normative field is produced by ferro-basalts showing high degrees of oxidation (both primary and secondary). If, however, the effect of the secondary oxidation is taken into account, this lobe would disappear, shifting down across the quartz–olivine boundary.

Similar composition plots on a silica/total alkali diagram (figure 10) also show the continuous spread from tholeiites through to the alkali field as defined by the Hawaiian division line of

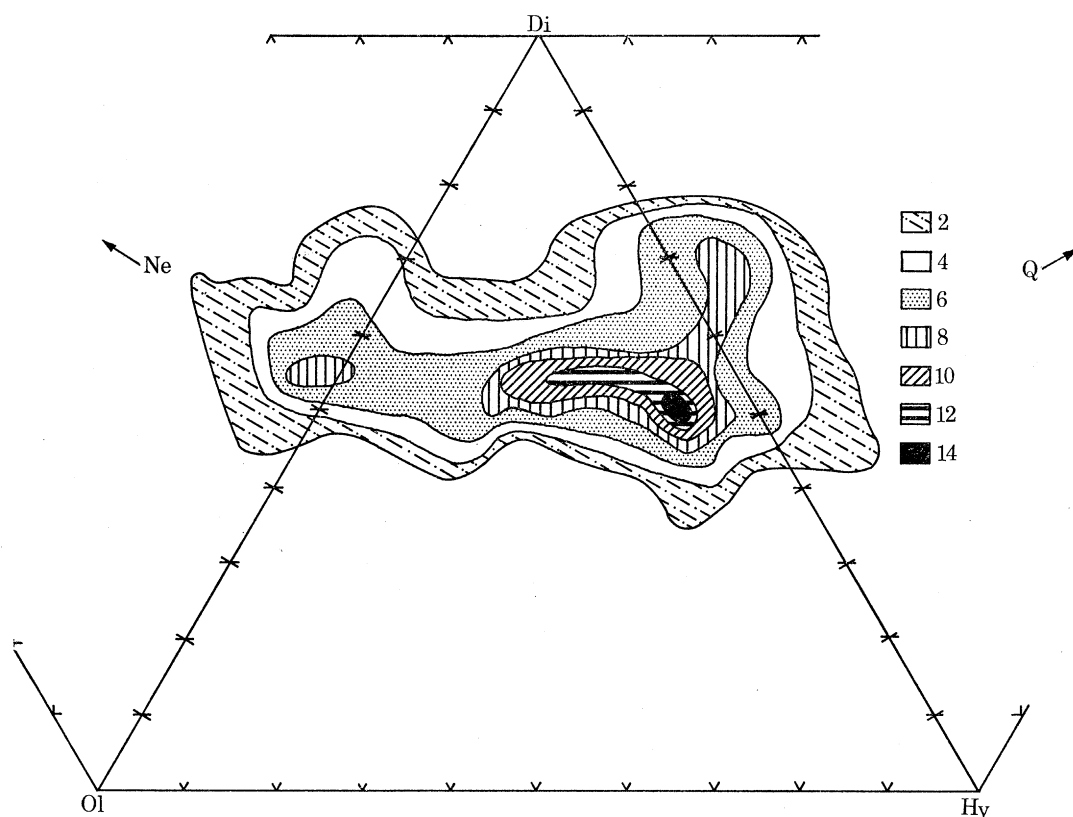FIGURE 9. Normative diagram Di–Hy–Ol–Q–Ne showing the statistical distribution of 60 basalt analyses from 45 °N expressed as a percentage of the 60 compositions. (Analyses after Muir & Tilley 1964; Aumento 1968, Aumento & Loncarevic 1969 and 25 new analyses by the Geological Survey of Canada.)
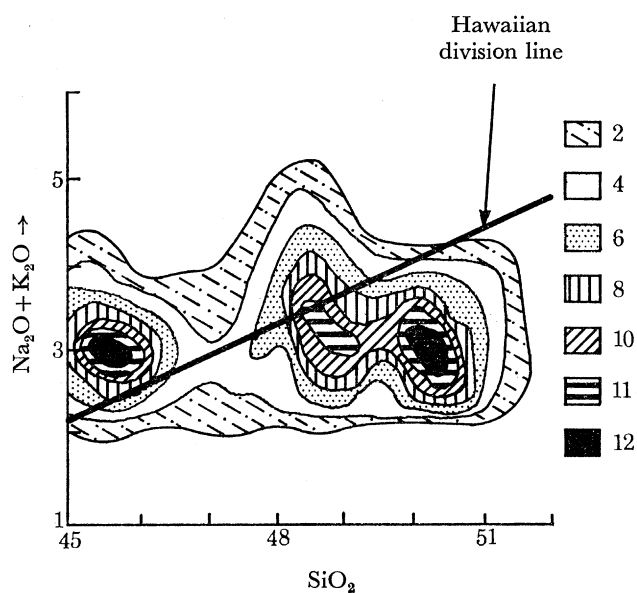


FIGURE 10. Silica/total alkali diagram showing the distribution of 60 basalt analyses from 45° N (as for figure 9).

Macdonald & Katsura (1964). In addition, the diagram illustrates three distinct fields of silica content. The first, between 45 and 46 % $SiO_2$, is composed primarily of ferro-basalts, and those basalts grading into diabase, whereas the other two, between 48.5 and 50.5 % $SiO_2$ contain the bulk of the basalts. Diabase and gabbro analyses were not used to construct the diagrams, but the former would appear to reinforce the peak at 45 to 46 % $SiO_2$ and the latter at 48.5 % $SiO_2$.
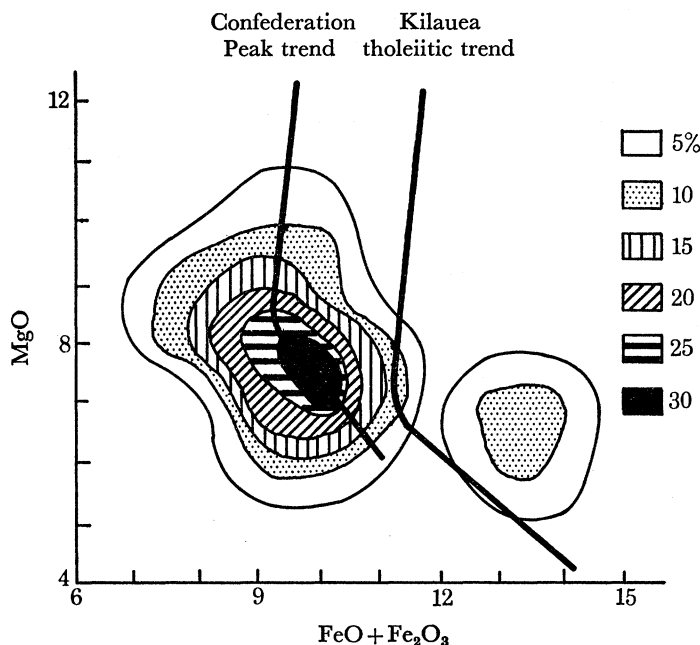


FIGURE 11. Magnesia/total iron diagram showing the distribution of 60 basalt analyses from 45° N (as for figure 9).

The distribution between the ferro-basalts and normal basalts is especially evident in the magnesia/total iron diagram of figure 11. The ferro-basalts are quite distinct from the others: most of them come from Bald Mountain (see Aumento & Loncarevic 1969), but additional examples have also been dredged from other block-faulted seamounts at 45° N. Most of the ferro-basalts have a subdiabasic texture, although in some instances pilotaxitic and fine-grained textures also occur. These basalts would appear to fall in the alkali field of figure 10 but in the normative diagram of figure 9 they are strongly quartz normative. The latter, as explained above, may be purely an effect of the secondary oxidation state of the iron content.

Aumento & Loncarevic (1969) considered the ferro-basalt to be late derivatives of the same parent magma as for the more normal basalts, which did not extrude onto the ocean floor, but crystallized within the walls of pre-existing fissure feeders.

The normal-iron basalts in figure 11 have a reasonable spread around the trend established for Confederation Peak (Aumento 1968). The spread could be reduced considerably by re-computing analysis after the effect of major concentration of calcic plagioclase xenocrysts are taken into account. The trend established both before and after recalculation of the analysis parallels the Kilauea tholeiitic trend, but shows a consistent displacement towards a lower total iron field.

Towards the beginning of the study at 45° N an attempt had been made to correlate basalt composition with depth: this was found to be possible when examining a single, undisturbed

seamount like Confederation Peak which consists largely of lava piles. There and in other similar examples it is possible to show that the first lavas to extrude are primarily tholeiites (these completely dominate the compositional range found on the floor of the Median Valley), whereas later cappings have more alkaline affinities. Similar correlations cannot be made readily on a regional scale, since most of the seamounts further from the axis of the Ridge are complicated by block faulting and later intrusive bodies, so that original layered attitudes and elevations are disturbed.

High alumina basalts occur randomly intermingled with both tholeiites and alkali basalts, and appear to have affinities with both basalt types. At this stage it is felt that the high-Al basalts do not exist as primary magmas, but are the result of partial or complete resorption of concentrations of high calcic plagioclase xenocrysts by both tholeiitic and alkali magmas.

### Basalt weathering

Dredge stations taken at distances greater than 30 km from the axis of the Mid-Atlantic Ridge unfortunately yielded heavily weathered material: only the inner cores of the larger dredged specimens were suitable for direct chemical, palaeomagnetic and isotopic analyses. However, an understanding of the chemical and mineralogical changes taking place on the ocean floor permits one to interpret to some extent data obtained from weathered specimens.

Weathering appears to affect neither crystallites nor phenocrysts, but only the glassy ground-mass interstitial to crystals, and the tachylitic crusts of the pillow lavas. The glass is hydrated and palagonitized, with the formation of clay minerals and various chlorites. Indeed, it has been possible to concentrate fresh phenocrysts from weathered basalts, and it may be possible in the future to use these concentrates for K/Ar age determinations.

Whole rock chemical changes due to ocean-floor weathering are quite severe, and distinct from the changes due to low grade metamorphism. The most marked variation is that of total water and the ferrous/ferric iron ratio. A plot of these two parameters (figure 12) shows that whereas fresh basalts fall predominantly in the region of 1 % $H_2O$ with a $Fe_2O_3/FeO$ ratio of 0.5, weathering increases both water and the iron oxidation ratio in a systematic way. Note the completely different field occupied by the low grade metamorphosed basalts. Since both water and iron oxidation ratio increases are so characteristic of weathering, either parameter may be used as a base against which to plot other variables.

The total water content was chosen in figure 13 to demonstrate variations in CaO and $Na_2O/K_2O$ with weathering. The peak at 11.5 % CaO for fresh basalts is hardly displaced on weathering, although there is a slight tendency for a loss of CaO on severe weathering. Similarly, although the $K_2O$ content increases on weathering, the $Na_2O/K_2O$ ratio remains reasonably constant with slight weathering (due to a slight gain in $Na_2O$) but tends to decrease on severe weathering due to a marked increase in $K_2O$. That these variations due to weathering are quite distinct from changes due to metamorphism is quite evident from figures 12 and 13.

Variations in the oxidation ratio of iron with weathering have important implications in the interpretation of palaeomagnetic data obtained from the basalts dredged. Irving, Robertson & Aumento (1969) have shown that whereas total iron content of these basalts shows no correla-tion with the specimen location, the $FeO/Fe_2O_3$ ratio has a marked peak (ratio = 10) at the Median Valley, tailing off symmetrically with increasing distance on either side of the axis of the Ridge to a low value of about 1.5 at a distance of 100 km from the axis. In contrast, although the natural remanent magnetization of the specimens also shows a peak on the Valley (1000 ×

FIGURE 12. Total water/iron oxidation ratio diagram showing the distribution of 60 basalt analyses and 15 greenstone analyses from 45° N (basalt analyses as for figure 9; greenstone analyses are from Aumento & Loncarevic 1969, and 10 new analyses by the Geological Survey of Canada).
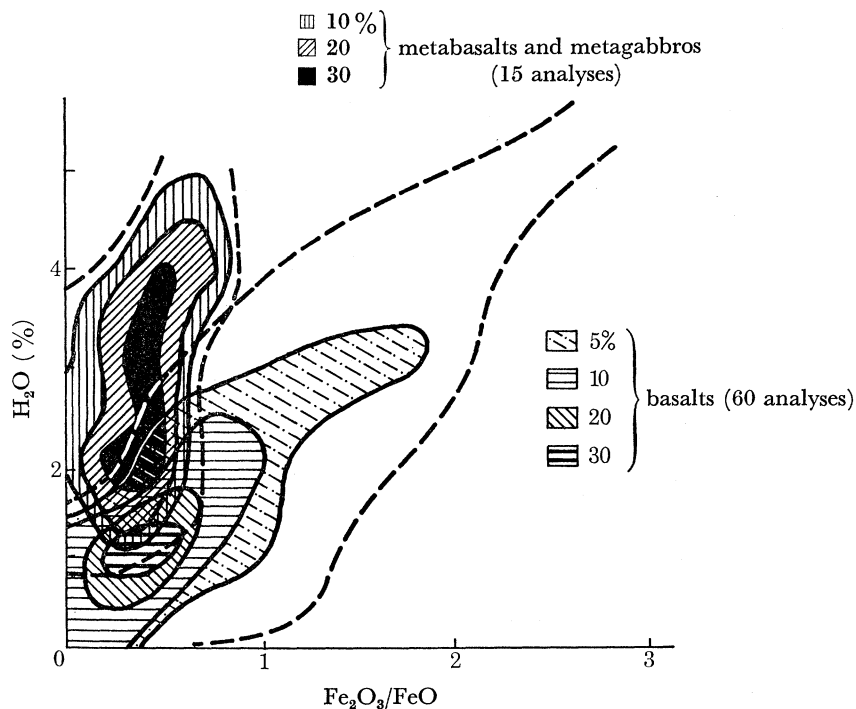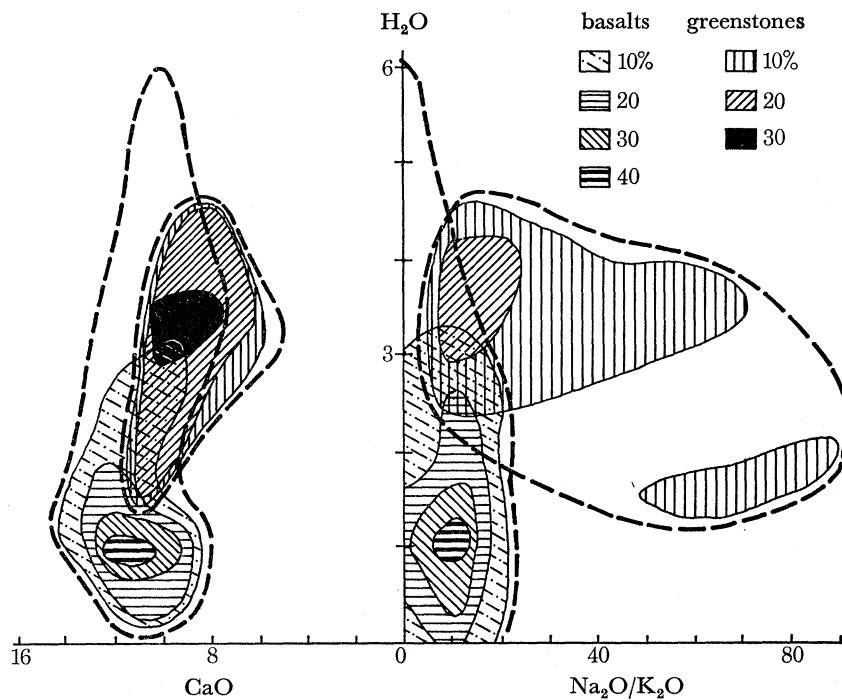
FIGURE 13. Total water/lime and total water/soda-potash ratio diagram showing the distribution of 60 basalt analyses and 15 greenstone analyses from 45° N (as for figure 12).

$10^{-4}$ cgs cm$^{-3}$) and falls off symmetrically with distance to $40 \times 10^{-4}$ cgs cm$^{-3}$, the intensity reduction is much more rapid, and the low values are reached within 20 to 30 km on either side of the axis.

Variations in remanent magnetization within one large specimen, the outside of which is highly weathered and the inside fresh, are less than variations between similar fresh specimens from a single dredge haul. Secondary (weathering) oxidation effects are therefore not the primary factors affecting the decay of remanent magnetization; weathered ocean-floor basalts may thus be suitable for palaeomagnetic investigations.

The increase in oxidation ratio with increasing distance from the axis is also reflected in oxygen isotopic studies of the basalts (K. Muehlenbachs, personal communication). Whereas fresh basalts have $\delta^{18}O/^{16}O$ values ranging from 5.63 to 6.61, there is a systematic increase in the ratio with distance from the axis, parallel to the increased oxidation state of the iron, up to values of 10 and greater. This is additional indication that this type of oxidation is a secondary effect due to reaction with cold, oceanic water, and has no bearing on oxidation due to low-grade metamorphism to be discussed in the next section.

## META-BASALTS AND META-DIABASES

### Lower grades of metamorphism

Basalts and diabases which have undergone low-grade metamorphism are very common throughout the area at 45° N. The lowest grades, of the zeolite facies, occur in intimate associa-tion with unmetamorphosed equivalents. It must be possible for this type of alteration to take place at very shallow depths of burial, possibly at the base of a single flow, for the crude sampling techniques used to succeed in obtaining specimens along lava flow exposures. Higher grades (greenschist facies) are restricted to fault scarps, but even these grades must have been produced at relatively shallow burial depths.

The most striking difference between ocean-water weathering and metamorphism proper is that the latter affects not only the glass and groundmass but also the phenocrysts. These show marked alteration and transformation to other mineral species. In the zeolite facies, the plagioclase phenocrysts are altered to analcite, whereas the groundmass and vesicles may contain zeolites in the series natrolite–mesolite–scolecite, as well as stilbite and heulandite. The higher grade greenschist facies rocks, while retaining their igneous textures and some relict phenocrysts of original composition, show alteration of calcic plagioclase to albite, augite to actinolite, olivine and glass to chlorite. Other minerals formed include epidote, tremolite, quartz, calcite, talc, titanian maghemite, and in the highest grades there also appears a strongly pleochroic green hornblende.

Metamorphism is accompanied by a major increase in total water content. However, as demonstrated in figure 12, the increase in water is not accompanied by an increase in oxidation ratio: the metamorphic (15 analyses) and the weathered basalts fall into two distinct fields. Oxygen isotopic analyses on the metamorphic basalts show no increase in the $\delta^{18}O/^{16}O$ ratio (ranging from 3.2 to 6.7) as had been seen in the weathering process, indicating that sea water is not the source for the water of metamorphism, but that a hot water of source similar to that of the basalts produces the hydration. Figure 13 shows that the addition of water is accompanied by a slight loss in CaO and a marked increase in the Na$_2$O/K$_2$O ratio. The latter is due both to K$_2$O loss and a Na$_2$O gain. Not demonstrated graphically, but associated with these changes,

are slight losses in $Al_2O_3$ and slight gains in $SiO_2$. Other major elements show changes either way, depending on individual cases.

Meta-basalts and meta-diabases of the grades described above occur both on the fault scarps forming the inner walls of the Median Rift Valley and on other fault scarps of seamounts further removed from the axis. In many cases, they can be shown to be overlain by fresh pillow basalts. The total vertical distance from the greenstone occurrences beneath to the pillow basalts above is of only 1000 m. If the exposures are the result of normal faulting without gravity sliding of the basalt layers then a maximum depth of burial of only 1000 m was available for the basalts to undergo metamorphism. Assuming there has been no gravity sliding of the volcanic layers, shallow burial in relatively short periods of time (the cliffs bordering the Median Rift Valley are not more than 700 000 years old) thus appears to be the basic requirement for the formation of these greenstones and greenschists. A steep thermal gradient producing temperatures in excess of 200 °C at a depth of 1 km beneath the Median Rift Valley is required by this metamorphic model. Irving *et al.* (1969), calculated from observed anomalies and from measurements of remanent magnetization and associated curie and blocking temperatures of basalts from the Median Rift Valley that temperatures in excess of 200 °C may be reached at depths shallower than 1 km. Palaeomagnetic evidence thus strongly supports the possibility of a high thermal gradient beneath the Median Rift Valley.

Metamorphism of the basalts has also been shown to destroy completely the original remanent magnetization of the basalts. The greenstones have very low remanent magnetization values and hence do not play an important part in the production of oceanic magnetic anomalies. Because of their shallow burial, they must occur somewhere at the base of oceanic layer 2: hence the magnetic anomalies are probably produced by the upper, unmetamorphosed part of layer 2. Indeed, the remanent magnetization of the pillow basalts at the top of layer 2 is so strong that only thin layers of pillows and shallow dykes are necessary to produce the magnetic anomalies observed.

### Higher grades of metamorphism

A number of localities beyond the immediate scarp slopes of the Median Rift Valley have yielded metamorphosed basic rocks ranging from the highest grades of the greenschist facies to the highest grades of the almandine amphibolite facies. These rocks are distinct from the greenstones described previously in that they have lost all igneous textures and relict minerals, and exhibit strong fabric lineations.

The amphibolites pose a problem concerning their origin. In many cases it is impossible to conclude whether they are locally derived rocks or are erratics ice rafted into the area by Pleistocene icebergs. These rocks are very angular and fresh, and often have little manganese coating on them: these are indications of a short exposure to sea water, but this may be due either to ice rafting or to recent outcropping by renewed block faulting of the seamounts. However, in a number of cases it is possible to decide on their origin, especially when they are manganese coated, have oxygen isotopic ratios similar to those of the basalts and meta-basalts and exhibit additional evidence for *in situ* occurrence.

Those rocks for which an *in situ* origin can be demonstrated are plotted in figure 8 as 'amphibolites', whereas the rocks of doubtful origin are grouped with the erratics; many of those of the latter may well be *in situ* also, but age determinations will be required to solve the problem.

Two distinct mineral assemblages have been encountered. The first, of the lower grade of the almandine amphibolite facies contains quartz, plagioclase in the range oligoclase-andesine

exhibiting bent twin lamellae, biolite, green pleochroic hornblende, epidote, sericitized orthoclase, magnetite and sphene. The rocks are gneissic, with well-developed mineral segregations forming conspicuous colour banding. One specimen shows a sharp contact between such an amphibolite and a lower grade greenstone: the latter still exhibits igneous flow textures across the gneissic texture of the amphibolite. The original basic rock was probably metamorphosed to an amphibolite and subsequently upthrusted, where it was intruded by a diabase. The two rocks were then subjected to lower grade metamorphism of the greenschis facies, which did not affect the amphibolite.

A higher degree of metamorphism produced the assemblage: hornblende, diopside (diallagic), plagioclase (oligoclase-andesine), sericitized orthoclase and minor biotite. These rocks may approximate the highest grades of the almandine amphibolite facies.

Rocks from both these metamorphic grades have suffered very little overall chemical alteration during metamorphism beyond that already discussed previously for the greenstones, except for a slight loss in total water. Therefore the higher grades of metamorphism are not associated with migration of elements, such as sodium and calcium for the greenstones, but take place in relatively sealed systems. However, the conditions of temperature and pressure have to be considerably higher than those for the greenstones. Minimum loads must be in the order of 4000 bar ($0.4 \, GN \, m^{-2}$), with temperatures of at least 550 °C. These conditions must be available at layer 3, some 6 km beneath sea level. Loads at such depths may be expected to be even greater under normal conditions, but the high temperatures must be produced by abnormally high heat flows.

## DIORITES

Diorites were recovered at station 159, on the eastern fault scarps of a seamount in the western High Fractured Plateau, and in minor amounts at stations 120 (from the same seamount) and 165 (see figure 14). Associated with the diorites were basalts, basalt breccias, serpentinized ultramafics and a number of ice-rafted erratics. Complete details of these rocks are available in Aumento (1969 a) and Plant, Aumento & Annels (1970), but they will be described here briefly.

Two main rock types, a dark type and a light type, can be distinguished among the samples collected, as follows:

### Melanocratic rocks

The dark rocks are medium to coarse-grained hornblende-rich quartz-diorites, with approximately 70 % plagioclase, 26 % hornblende, 4 % quartz and less than 1 % sphene, ores and accessory minerals. Hornblende is of a dark green pleochroic variety. The plagioclases are twinned and zoned with shadowy oscillations from clear zones of andesine ($An_{40-45}$) in a low temperature structural state to slightly cloudy rims of oligoclase ($An_{15}$). The plagioclase and hornblende crystals are rarely seen to be moulded onto one another, and this feature, together with the high proportion of plagioclase in the rock, is taken to indicate that the two minerals are cumulus phases of near simultaneous precipitation. The euhedral habit of the hornblendes is particularly striking and would appear to negate an origin for hornblende by replacement of clinopyroxene.

However, one anhedral grain of pale green clinopyroxene was found in the sections examined; the clinopyroxene bears a broad rim of dark green hornblende similar in composition to that of the independent hornblende crystals in the rock. This pyroxene grain is interpreted as being a xenocryst (possibly cognate) on which a reaction rim has developed.

A few of the hornblende prisms are replaced by foxy-red biotite blades; such replacement is not common, since more often prisms are replaced by a pale green chlorite. Grids of acicular sphene lie parallel to the chlorite fibres. Isolated euhedral apatite and zircon are scattered throughout. The opaque oxide minerals are of early precipitation, the smallest grains being frequently enclosed by the early precipitated plagioclase and hornblende crystals.
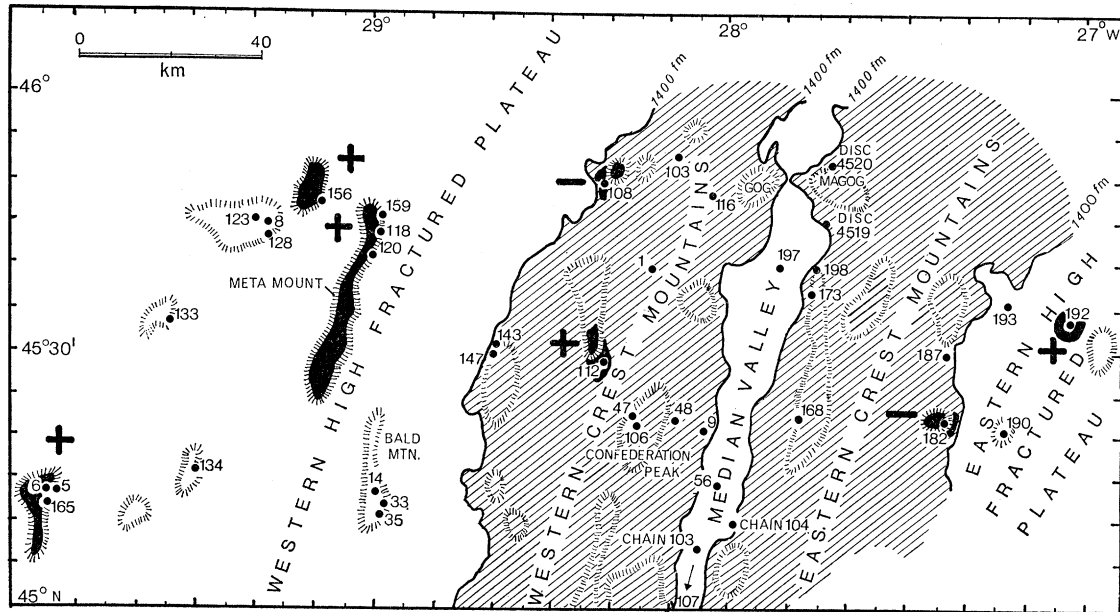


FIGURE 14. Schematic bathymetry of the area at 45° N showing the major morphological features; the locations of the stations yielding serpentinized ultramafics and diorites and the signs of the associated magnetic anomalies are superimposed; also shown are the 42 dredge stations from which fission track and ferro-manganese dates were established.

Small dark patches of three different mineralogies were found in the dark rocks. These include: (1) amphibole-rich patches, with ovoid to tear-shaped outlines, composed of fine-grained plagioclase and green hornblende. These patches are similar in appearance and chemistry to the metamorphic amphibolites described previously; (2) ultrabasic patches, also ovoid, composed of enstatite and olivine altered to goethite, talc and serpentine. These patches are surrounded by coronas of hornblende and mica; (3) rounded patches of serpentine, representing original serpentinous or olivine-rich material which subsequently underwent deuteric alteration.

### Leucocratic rocks

The light rocks may be classified as trondhjemites or albite granites. They contain 42 % plagioclase, 5 % hornblende, 2 % biotite, 25 % quartz, 2 % opaques and epidote, and 24 % of an intergrowth of albite with K-feldspar. The maximum core composition of the plagioclases lies in the oligo-class range $(An_{20})$, whereas margins reach $An_5$. These crystals are commonly bordered by a cloudy feldspar in which are developed variable amounts of thin lamellar alterations of pure K-feldspar and pure albite which trend perpendicular to the plagioclase boundaries. These lamellae are in optical continuity with the plagioclase crystals, but at the same time tend to fill in the interstices between the plagioclase and surrounding crystals.

The diorites analysed show consistently high soda content (5.5 %), and unusually high soda/potash ratios. Silica content varies from 50 % in the melanocratic rocks to 72 % in the

leucocratic ones. A plot of their composition on an $FeO–MgO–Na_2O–K_2O$ diagram (figure 15) shows strong similarities between the M.A.R. trend and those of the Oregon and Troodos alpine ultramafic complexes (Thayer & Himmelberg 1968). Their chemistry, therefore, and the albite/K-feldspar borders on some of the plagioclases, are reminiscent of the albitized diorites of alpine ultramafic intrusive complexes. By association, therefore, these diorites are thought to be the product of residual magmatic liquids intruded at a late stage into serpentinite bodies: the rising magmas may have incorporated xenoliths of the country rock (amphibolites, peridotites or serpentinites) through which they were intruded.
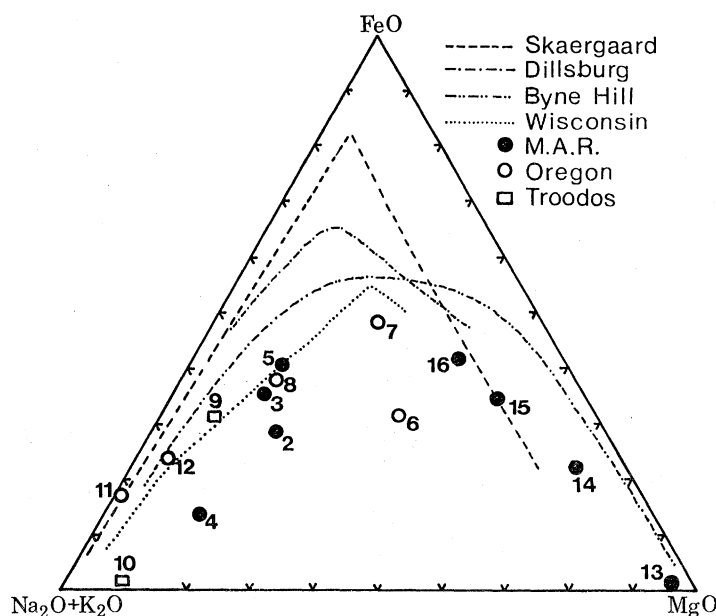


FIGURE 15. Iron/magnesia/total alkali variation diagrams showing the M.A.R. trend from serpentinites (13, average of 10 analyses) through to gabbro (14), diabase (15), basalt (16, average of 25 analyses), quartzy diorite (2, 3, 5) and trondhjemite (4), compared to rocks from Oregon (quartz-diorite 6 and 7, partlalbitized quartz-diorite 8, albite granite 11 and 12) and from Troodos (hornblende trondhjemite 9 and quartz-albite microporphyry 10). After Plant *et al.* (1970) and Thayer & Himmelberg (1968).

## SERPENTINIZED ULTRAMAFICS

Figure 14 shows the spatial distribution of serpentinized ultramafic rocks at 45° N. It is evident that the serpentinites are absent from the Median Valley, its immediate scarp slopes and first range of Crest Mountains, but appear only beyond some 30 km from the axis of the Ridge, When they do occur, however, their occurrence bears no relation to topography: serpentinites have been dredged from tops of seamounts, from lower down steep slopes, from the base of cliffs, and from relatively flat-lying areas. Hence they may outcrop at any elevation on the sea floor, quite unrelated to the presumed crustal stratigraphy. On the other hand, whereas most seamounts do not have direct correlations with magnetic anomalies above them, the serpentinite occurrences always fall beneath strong positive or negative anomalies, as indicated in figure 14, whether they be on seamounts or on valley floors. Irving *et al.* (1969) have shown that the serpentinites at 45° N have very strong remanent magnetization and magnetic susceptibility values, so that one would expect considerable magnetic field disturbances to be produced by large masses of serpentinites close to the sea floor.

The random elevation of the occurrence of serpentinites, unlike the well-controlled stratigraphic occurrence of basalts, diabases, gabbros and metamorphic basic rocks suggests that the serpentinites which occur on the sea floor were emplaced tectonically through the basic stratigraphy of layers 2 and 3 of the oceanic crust. These ultramafic serpentinized bodies may have the form of diapiric intrusions, much like the alpine-type continental occurrences. Their notable absence from the Median Valley and immediate areas is also interesting, since this area is relatively undisturbed by complex faulting, whereas their presence in the more disturbed terrains further removed from the axis may have tectonic implications. Intrusion and faulting may be related and dependent on one another in some way.

Both strongly sheared, fractured serpentinites and completely undisturbed specimens have been recovered. The latter, although more than 90% serpentinized, allow a study of original textures and mineralogy to be made.

The undisturbed specimens occur primarily from one locality, at stations 5, 6 and 165 (see figure 14) the extreme southwest of the area. The slope sampled was the steep eastern fault scarp of the seamount, and serpentinites, together with minor diorites, were recovered more than half way up the slope. Original, pre-serpentinization rock types include harzburgite, chromite harzburgite, gabbro, troctolitic gabbro, dunite, and rare lherzolite. The harzburgite is especially massive with original minerals up to 4 mm in grain size. Some specimens show gradation within a few centimetres (and sharp contacts as well) from harzburgite to dunite, from harzburgite to a chromite harzburgite to a troctolite, or directly from harzburgite to gabbro. Textures show crude gravity cumulative features, and the diversity of rock types collected over short dredge haul distances suggest that the original ultrabasic complex must have approximated a pseudostratiform mass.

Serpentinization of the ultramafics from station 5, 6 and 165, although very thorough, did not disturb the original igneous structures. Table 2 attempts to condense the X-ray mineralogy of the M.A.R. serpentinites as studied from both serpentine mineral concentrates and whole rocks. Brucite is conspicuous in its absence; also notable are the high magnetite content (intimately dispersed within the serpentine minerals, such that it could not be separated magnetically) and the overwhelming presence of lizardite above all other serpentine group minerals. The cell parameters of lizardite were measured accurately by X-ray diffractometry, and were found to be consistently smaller than for lizardites from the alpine-type intrusives.

Some of the coarse (9 mm grain size) gabbros and troctolites from station 165 have also formed a massive, extremely fine grained milky white rock instead of a serpentinite. X-ray diffraction analyses of the milky white product have shown it to be an intimate admixture of hydrogrossular, prehnite, epidote, chlorite and zeolites. Such a mixture is characteristic of the rodingite association common of the alpine-type ultramafic bodies.

Serpentinites from other dredge stations are characterized by varying degrees of brecciation and shearing. Two localities (159 and 182) have yielded cataclastic amphibole-bearing peridotites with textures and minerology similar to those described from St Peter and St Paul's rocks (Melson, Jarosewich, Bowen & Thompson 1967: Tilley 1947). However, harzburgites predominate both at these localities and elsewhere. Original mineral grains range from 2 to 4 mm. Multiple stages of deformation and serpentinization are evident: in general the cataclastic structure produced is composed of a completely serpentinized matrix enclosing very fresh ultramafic rock fragments. The latter contain fresh orthopyroxenes, olivine (and amphibole in the amphibole peridotites) and rare clinopyroxenes. There is strong mineral layering, some

of which is original magmatic cumulate layering, but there is also layering due to later mechanical processes superimposed onto the original magmatic layering, possibly accentuating the latter.

TABLE 2. X-RAY MINERALOGY OF SERPENTINE MINERAL CONCENTRATES AND WHOLE ROCK POWDERS FROM SERPENTINIZED ULTRAMAFICS FROM THE MID-ATLANTIC RIDGE AT 45° N

| sample (AG–68–) | chrysotile | antigorite | lizardite | brugnatellite | brucite | chlorite | talc | biotite | olivine | clinopyroxene | enstatite | tremolite | magnetite | carbonate |
|---|---|---|---|---|---|---|---|---|---|---|---|---|---|---|
| 6–1 serp. conc. | — | — | xx | — | — | — | — | — | — | — | tr. | — | — | — |
| 6–1 wh. rock | — | — | xx | — | — | tr. | — | — | — | — | tr. | — | tr. | — |
| 6–5 serp. conc. | — | — | xx | — | — | — | — | — | — | — | — | — | — | — |
| 6–5 wh. rock | — | — | xx | — | — | tr. | — | — | — | tr. | — | tr. | — | x |
| 6–7 wh. rock | — | — | xx | — | — | tr. | — | — | — | — | tr. | — | — | — |
| 165–1 serp. conc. | — | — | xx | — | — | — | — | — | — | — | — | — | — | — |
| 165–1 wh. rock | — | — | xx | — | — | — | tr. | tr. | tr. | — | — | — | — | — |
| 165–2 serp. conc. | x | — | xx | — | — | — | — | — | — | — | — | — | — | — |
| 165–2 wh. rock | x | — | xx | — | — | — | — | — | tr. | — | — | — | — | — |
| 165–8 serp. conc. | — | — | xx | — | — | x | — | — | — | — | — | — | — | — |
| 165–8 wh. rock | — | — | xx | — | tr. | x | — | — | — | tr. | tr. | — | — | — |
| 165–13 wh. rock | — | — | xx | — | tr. | tr. | — | — | tr. | — | tr. | — | tr. | — |
| 165–14 wh. rock | — | — | xx | tr. | — | tr. | — | — | tr. | — | — | — | x | — |
| 165–16 wh. rock | — | — | xx | — | — | tr. | — | — | tr. | — | tr. | — | x | — |
| 165–17 wh. rock | — | — | xx | tr. | — | x | — | tr. | — | — | tr. | — | x | — |
| 165–50 wh. rock light | — | — | xx | — | tr. | x | — | — | tr. | — | tr. | — | — | — |
| 165–50 wh. rock dark | — | — | xx | tr. | — | x | — | tr. | tr. | — | tr. | — | x | — |
| 108–3 serp. conc. | — | — | xx | — | — | — | — | — | — | — | — | — | — | — |
| 108–3 wh. rock | — | — | xx | — | — | — | — | — | tr. | — | — | — | — | — |
| 112–1 serp. conc. | — | — | xx | — | — | tr. | — | — | — | — | — | — | — | — |
| 112–1 wh. rock | — | — | xx | — | — | x | — | — | tr. | — | tr. | — | tr. | — |
| 156–10 serp. conc. | — | — | xx | — | — | — | tr. | — | — | — | — | — | — | — |
| 156–10 wh. rock | — | — | xx | — | — | — | — | — | — | — | — | tr. | — | — |
| 159–10 serp. conc. | x | — | xx | — | — | — | tr. | — | tr. | — | — | — | — | — |
| 159–10 wh. rock | x | — | xx | — | — | tr. | tr. | — | tr. | — | — | x | x | x |
| 182–1 serp. conc. | — | — | xx | — | — | — | — | — | — | — | — | tr. | — | — |
| 182–1 wh. rock | — | — | xx | — | tr. | x | — | — | tr. | — | tr. | x | — | x |
| 192–1 serp. conc. | — | x | xx | — | — | x | x | — | tr. | — | tr. | tr. | — | — |
| 192–1 wh. rock | — | x | xx | — | — | x | x | — | tr. | tr. | x | tr. | — | — |
| 192–3 serp. conc. | x | — | xx | — | — | x | x | — | — | — | — | — | — | — |
| 192–3 wh. rock | x | — | xx | — | — | x | x | — | tr. | — | tr. | — | — | x |
| 192–5 wh. rock | — | — | xx | — | — | tr. | x | — | tr. | — | tr. | — | tr. | — |

*Note.* serp. conc., serpentine concentrate; wh. rock, whole rock 'as is'; xx, major concentrations; x, minor concentrations; tr., trace concentrations.

Sixty individual chrome spinel grains concentrated from nineteen serpentinite specimens (including all the ultramafic rock types found) were analysed with an electron probe and results were plotted in figure 16, after Irvine (1967). Irvine had demonstrated that chrome spinels from alpine intrusions formed a different compositional field to those from layered intrusions, and as such could be used as petrogenetic indicators. The M.A.R. chrome spinels plot in a particularly tight field which overlaps both the alpine and stratiform fields, and hence does not assist in confirming affinities of the Ridge specimens with either type of continental intrusion. They do, however, stress the transitional nature of the Ridge ultramafics.

As an additional attempt to establish affinities for these rocks, the complete mineralogy of the M.A.R. serpentinites is tabulated in table 3 against those of the layered Muskox intrusions and the alpine-type Quebec deposits of Jeffrey Mine, Eastern Townships and Mt Albert,
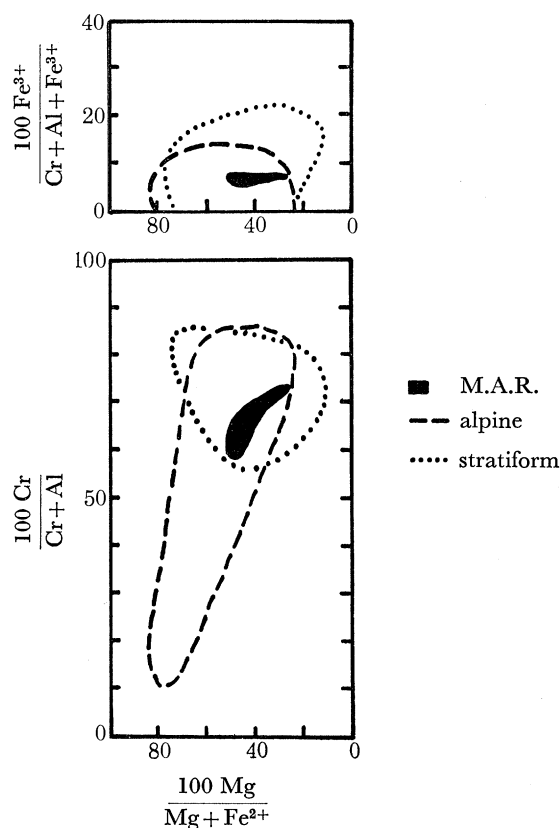


FIGURE 16. Chrome spinel compositions from the M.A.R. ultramafics (60 analyses) compared to the distribution fields of chrome spinels from continental alpine and stratiform intrusions. After Irving (1965, 1967).

TABLE 3. COMPARATIVE X-RAY MINERALOGY OF SERPENTINIZED ULTRAMAFICS FROM THE MID-ATLANTIC RIDGE, THE MUSKOX LAYERED INTRUSION, AND THE ALPINE-TYPE JEFFREY MINE AND MT ALBERT INTRUSIONS FROM QUEBEC, CANADA

| | degree of serpentiniza-tion | inferred temperature of serpentiniz-ation/°C | olivine composition (% Fo) | lizardite % | lizardite cell parameters | brucite | chlorite |
|---|---|---|---|---|---|---|---|
| M.A.R. | > 90 % | ~ 485 | 81–87 | 92.6 | smallest | 0.2 | 2.0 |
| Muskox | 40–90 | ⩽ 485 | 80–85 | 87.5 | ↓ | 1.5 | 1.4 |
| Jeffrey Mine | 60–80 | ~ 400 | 90–93 | 95.3 | | 2.2 | 0.6 |
| Mt Albert | 60–80 | ⩽ 400 | 91–93 | 83.1 | largest | 3.7 | 1.7 |

| | talc | biotite | olivine | clino-pyroxene | enstatite | tremo-lite | magne-tite |
|---|---|---|---|---|---|---|---|
| M.A.R. | 1.0 | 0.2 | 0.6 | 0.2 | 0.8 | 0.7 | 1.5 |
| Muskox | — | 2.0 | 1.1 | 0.7 | — | — | 2.9 |
| Jeffrey Mine | 0.2 | — | 0.3 | — | 0.3 | — | — |
| Mt Albert | 1.6 | — | 3.9 | — | 2.7 | 1.8 | — |

Gaspè. The strongest similarities are between M.A.R./Muskox and Jeffrey Mine/Mt Albert. The mineralogy suggests that the first group of intrusions was serpentinized close to the maximum temperature of serpentinization (close to 485 °C), and the second group under considerably cooler conditions (400 °C or less). Aumento (1969c) suggested that differences in temperatures of serpentinization reflected both the variations in sizes, and hence the rates of cooling, of the intrusions, and the times at which serpentinization took place relative to emplacement. In the alpine-type intrusives serpentinization probably occurred contemporaneously with the emplacement of a cool, semicrystalline ultrabasic mass, whereas in the stratiform intrusives serpentinization probably occurred on cooling after emplacement and after termination of the process of differentiation by crystal settling. On the M.A.R. it is thought that magmatic differentiation took place deep beneath the floor of the Median Rift Valley, and that incipient serpentinization took place there under hot conditions on completion of the crystallization process, much like in a large layered intrusion. Subsequently upthrusting of large blocks associated with sea-floor spreading mobilized the partly serpentinized ultramafics and intruded them into the overlying volcanic and hypabyssal sequences. These tectonic processes were probably accompanied by renewed serpentinization, which, due to the size of the bodies and proposed high heat flow of the area, took place at relatively high temperatures. Repeated upthrusting finally exposed both the serpentinite diapirs and any undisturbed but serpentinized differentiated ultrabasic layers (e.g. seamount at stations 5, 6, 165). This would explain why ultrabasics are not found on the fault scarps of the Median Rift Valley (where throws of up to 1000 m expose gabbros and greenstones only) but are common, (in association with amphibolites and diorites) on repeatedly faulted blocks further removed from the axis.

Such a tectonic model may explain why certain characteristics of M.A.R. serpentinites have affinities with those of layered intrusives, whilst others are more akin to alpine-type intrusives.

## Erratics

Almost a quarter of the specimens collected (23 %) are gneissic, granitic and sedimentary rocks showing rounding, polishing, striations and lack of weathering. Whenever dredge hauls contained appreciable concentrations of these rock types, they were found to be petrologically unrelated to one another, and were characteristically lacking in, or had very thin coatings of, ferro-manganese crust, indicative of relatively brief contact with ocean waters. These rocks have been interpreted as being erratics ice rafted from the continents during Pleistocene ice ages.

K–Ar age determinations on some of these rocks have given middle Precambrian ages (Aumento & Loncarevic 1969) completely outside the limits suggested by the ages of the associated basalts (Fleisher et al. 1968; Aumento 1969b) and by current sea-floor spreading hypotheses. The dates further support a possible ice rafted origin.

A preliminary study of the distribution of erratics indicates that they are completely absent on the Median Valley floor, that they are scarce in the mountain ranges immediately flanking the valley, but beyond these areas they are abundant and randomly distributed over the whole area (Paterson 1970). Such a distribution may be the result of ocean-floor spreading, indicating that the Median Valley is younger than the last ice age, or that extrusions subsequent to the last ice age have engulfed any erratics present in the Median Valley, making them irretrievable by ordinary dredging methods.

Paterson has attempted to date the time of deposition of glacial erratics at 45° N by measuring the maximum ferro-manganese coating thickness on every erratic specimen and plotting the thicknesses on histograms. By further knowing the rate of ferro-manganese deposition in the area from an independent source (Aumento 1969 *b*), he was able to date the peaks obtained on his histograms. The majority of erratics have very thin coatings and appear to have been deposited during the last major period of Pleistocene glaciation, the Visconsin, some 60 ka ago. Additional histogram peaks can be correlated with the Illinoian Glacial (450 ka ago) and the Kansas Glacial (more than 1 Ma ago) periods. These correlations depend on two criteria: that the rate of ferro-manganese deposition is constant over long periods of time, and that the specimens collected were not buried by foraminiferal muds, otherwise the ferromanganese clock would be halted, resulting in erroneously young ages.

### AGE DETERMINATIONS AND SPREADING RATES

Four basalts and a hornblende concentrate from the diorites of station 159 were dated by K–Ar techniques (Muir & Tilley 1964; Aumento *et al.* 1968; Aumento 1969 *a*); eleven basaltic glasses were dated by fission track methods (Fleischer *et al.* 1968; Aumento 1969 *b*); in addition the minimum ages for each of the 42 dredge station localities were inferred by measuring the maximum ferro-manganese coating on all the specimens and correlating the thicknesses found with previously calibrated depositional rates.

Results from the independent K–Ar and fission track dates and from the relative ferromanganese method are given in figure 17. They all concur that:

(1) A mechanism for ocean floor spreading from a central axis is active in the area.

(2) The Median Valley floor is very young, always less than 100 ka, and often considerably younger.

(3) The Crest Mountains to the west of the Median Valley have been spreading at a rate of between 2 and 4 cm $a^{-1}$, suggesting that the whole Crest Mountains region is less than 2 Ma old.

(4) The High Fractured Plateau region is much older, and its average spreading rate, calculated with the current M.A.R. axis as the origin, is between 0.6 and 1.2 cm $a^{-1}$, less than half the rate found on the Crest Mountains. On the other hand, the High Fractured Plateau/ Crest Mountains morphological boundary (which was probably the axis of spreading 2 Ma ago if statement (3) above is correct) can be used as the origin (centre of spreading); this gives not the average spreading rate over the last 16 Ma but the actual rate in the period 2 to 16 Ma ago; this actual rate of spreading is of only 0.4 to 0.6 cm $a^{-1}$.

(5) The change in spreading rate is coincident with the physiographic boundary between the Crest Mountains and the High Fractured Plateau. This boundary has also tectonic implications: the former region shows relatively few fractures and scarce ultramafic intrusions, while the latter is highly fractured both parallel and at right angles to the Ridge axis, and is rich in diapiric ultramafic intrusions.

The spreading rate away from the Ridge axis (and thus an inferred age of the crustal rocks), can also be calculated by correlating the observed magnetic profile with a theoretical model (Vine 1966). Although in many oceanic areas spreading rates can be calculated from single profiles (Le Pichon 1968), this method cannot be applied directly in the North Atlantic, presumably because of a slow rate of spreading (Matthews 1967).

The systematic surveys at 45° N enabled Loncarevic & Parker (1970) to construct an average magnetic profile by projecting 53084 magnetic observations onto a line perpendicular to the strike of the Ridge. Their conclusion was that the spreading rate for the last 10 Ma has been constant and slightly different for the eastern and western limbs of the Ridge (1.10 and
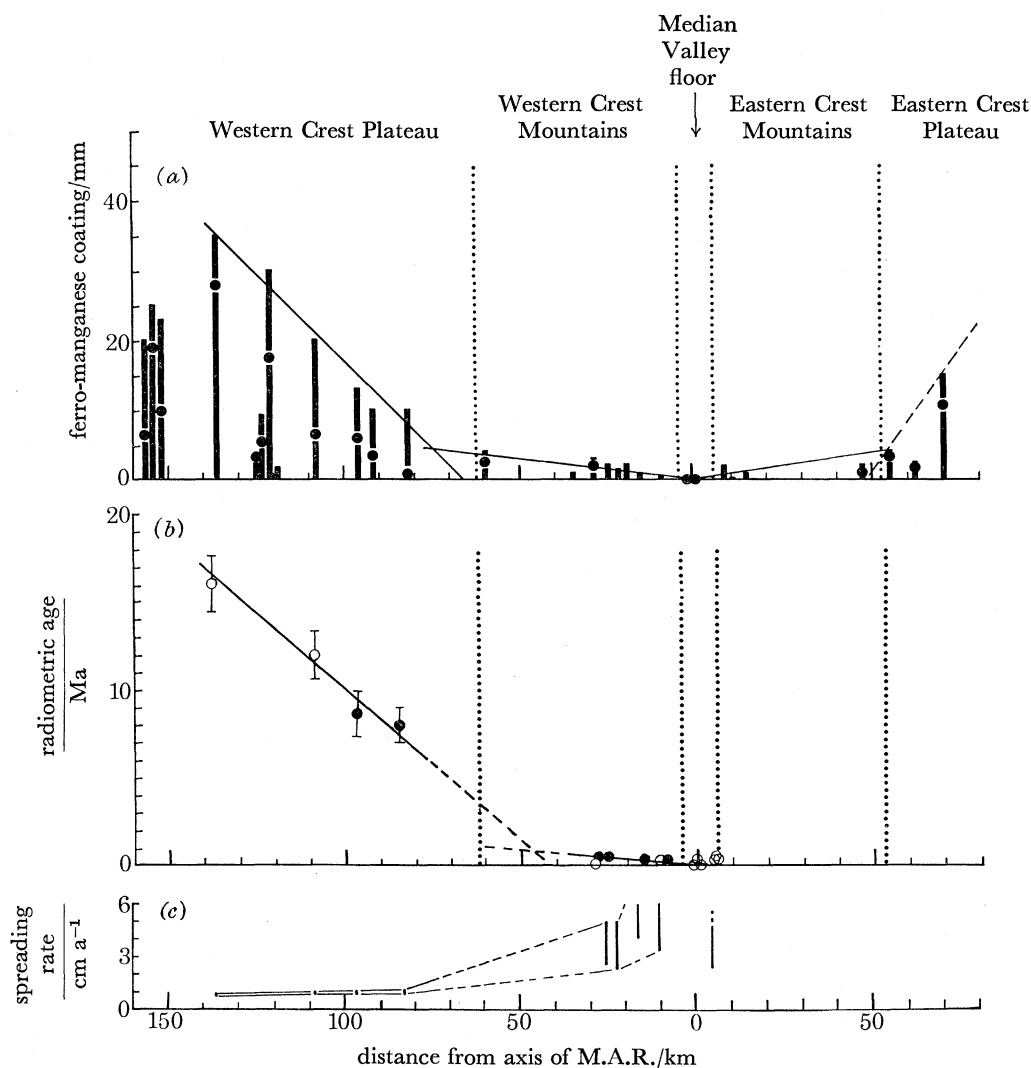


FIGURE 17. (a) maximum ferro-manganese coating thicknesses and (b) ○, fission track and ●, K–Ar dates (and (c) spreading rates computed from these) on basalts plotted against distance from the axis of the M.A.R. at 45° N.

1.28 cm a⁻¹ per limb respectively). This finding is at variance with that observed from direct age determinations of rock specimens, as discussed above (Aumento 1969b). If it is assumed that the specimens sampled were injected into the crust at the axis of the Ridge, the radiometric dates then support the hypothesis of two rates of spreading.

However, Loncarevic & Parker (1970) thought it unlikely that the tectonic plate moving away from the Ridge axis has the full strength throughout its thickness right up to the edge near the axis. Indeed as this edge grows by accretion of newly injected material it is probably wedge shaped (note the seismic evidence for a thickening of layer 3 away from the axis) and only

gradually reaches the full strength at some distance from the axis. The weaker section near the axis could possibly allow later volcanic activity to take place. If this younger material is then sampled, it would yield erroneously faster spreading rates.

## CONCLUSIONS

Detailed geological–geophysical investigations over a restricted area of the Mid-Atlantic Ridge have demonstrated that a single area, when sampled adequately, can provide most of the rock types and geological settings found elsewhere at widely scattered localities throughout the mid-oceanic ridges. In addition, unsuspected oceanic occurrences of igneous rocks characteristic of continental environments have also been found.

These investigations negate the older ideas for simple geological settings of the oceanic crust; the latter were based on insufficient sampling. New evidence suggests that the ocean floor approximates the complexities found on continental environments.

## REFERENCES (Aumento *et al.*)

Aumento, F. 1968 The Mid-Atlantic Ridge near 45° N. II. Basalts from the area of Confederation Peak. *Can. J. Earth Sci.* **5**, 1–21.

Aumento, F. 1969a Diorites from the Mid-Atlantic Ridge at 45° N. *Science, N.Y.* **165**, 1112–1113.

Aumento, F. 1969b The Mid-Atlantic Ridge near 45° N. V. Fission track and ferro-manganese chronology. *Can. J. Earth Sci.* **6**, 1431–1440.

Aumento, F. 1969c Serpentine mineralogy of ultrabasic intrusions in Canada and on the Mid-Atlantic Ridge. *Geol. Surv. Can. Pap.* **69–53**, 1–67.

Aumento, F. 1970 Improved positioning of dredges on the sea floor. *Can. J. Earth Sci.* **7**, 534–539.

Aumento, F., Wanless, R. K. & Stevens, R. D. 1968 Potassium–Argon ages and spreading rates of the Mid-Atlantic Ridge at 45° N. *Science, N.Y.* **161**, 1338–1339.

Aumento, F. & Loncarevic, B. D. 1969 The Mid-Atlantic Ridge near 45° N. III. Bald Mountain. *Can. J. Earth Sci.* **6**, 11–23.

Carmichael, C. 1970 The Mid-Atlantic Ridge near 45° N. VII. Magnetic properties and opaque mineralogy of dredged samples. *Can. J. Earth Sci.* **7**, 239–256.

Fleischer, R. L., Viertl, J. R. M., Price, P. B. & Aumento, F. 1968 Mid-Atlantic Ridge, age and spreading rates. *Science, N.Y.* **161**, 1339–1342.

Garner, D. M., & Ford, W. L. 1969 The Mid-Atlantic Ridge near 45° N. IV. Water properties in the Median Valley. *Can. J. Earth Sci.* **6**, 1359–1363.

Irvine, T. N. 1965/7 Chromian Spinel as a petrogenetic indicator. I and II. *Can. J. Earth Sci.* **2**, 648–672; **4**, 71–103.

Irving, R., Robertson, W. A. & Aumento, F. 1969 The Mid-Atlantic Ridge near 45° N. VI. Remanent intensity, susceptibility and iron content of dredged samples. *Can. J. Earth Sci.* **7**, 226–238.

Keen, C. & Tramontini, C. 1969 A seismic refraction study on the Mid-Atlantic Ridge. *Geophys. J.* (in the Press.)

Keen, M. J. & Manchester, K. S. 1969 The Mid-Atlantic Ridge near 45° N. X. Sediment distribution and thickness from seismic reflection profiling. *Can. J. Earth Sci.* **7**, 735–747.

Le Pichon, X. 1968 Sea floor spreading and continental drift. *J. Geophys. Res.* **73**, 3661–3697.

Loncarevic, B. D. 1969 Buoy plot as a survey aid. *Trans. Appl. Sea-going Computers Symp.*, pp. 27–33. Washington, D.C.: Mar. Tech. Soc.

Loncarevic, B. D., Mason, C. S. & Matthews, D. H. 1966 The Mid-Atlantic Ridge near 45° N. I. The Median Valley. *Can. J. Earth Sci.* **3**, 327–349.

Loncarevic, B. D. & Parker, R. L. 1970 The Mid-Atlantic Ridge near 45° N. XV. Magnetic anomalies and sea-floor spreading. *Can. J. Earth Sci.* (in the Press.)

Macdonald, G. A. & Katsura, T. 1964 Chemical composition of Hawaiian lavas. *J. Petrology* **5**, 83–133.

Matthews, D. H. 1967 Studies of the Atlantic deep-sea floor. *Chall. Soc.* **3**, 28–38.

Matthews, D. H. & Bath, J. 1967 Formation of magnetic anomaly patterns of Mid-Atlantic Ridge. *Geophys. J. R. astr. Soc.* **13**, 349–357.

Melson, W. G., Jarosewich, R., Bowen, V. T. & Thompson, G. 1967 St Peter and St Paul Rocks: A high-temperature, mantle-derived intrusion. *Science, N.Y.* **155**, 1532–1535.

Muir, I. D. & Tilley, C. E. 1964 Basalts from the northern part of the rift zone of the Mid-Atlantic Ridge. *J. Petrology* **5**, 409–434.

Paterson, I. S. 1970 The Mid-Atlantic Ridge near 45° N. XVI. Pleistocene glacial erratics. *Can. J. Earth Sci.* (in the Press.)

Pitman, W. C., Herron, E. M. & Heirtzler, J. R. 1968 Magnetic anomalies in the Pacific and sea floor spreading. *J. Geophys. Res.* **73**, 2069–2085.

Plant, A. G., Aumento, F. & Annels, R. 1970 The Mid-Atlantic Ridge near 45° N. XVII. Diorites with alpine affinities. *Can. J. Earth Sci.* (in the Press.)

Thayer, T. P. & Himmelberg, G. R. 1968 Rock succession in the alpine-type mafic complex at Canyon Mountain, Oregon. *23rd Int. Geol. Congr.* **1**, 175–185.

Tilley, C. E. 1947 The Dunite–Mylonites of St Paul's Rocks. (Atlantic.) *Am. J. Sci.* **246**, 483–491.

Vine, F. J. 1966 Spreading of the ocean floor: new evidence. *Science, N.Y.* **154**, 1405–1415.

# Petrology of submarine volcanics from the NE Pacific
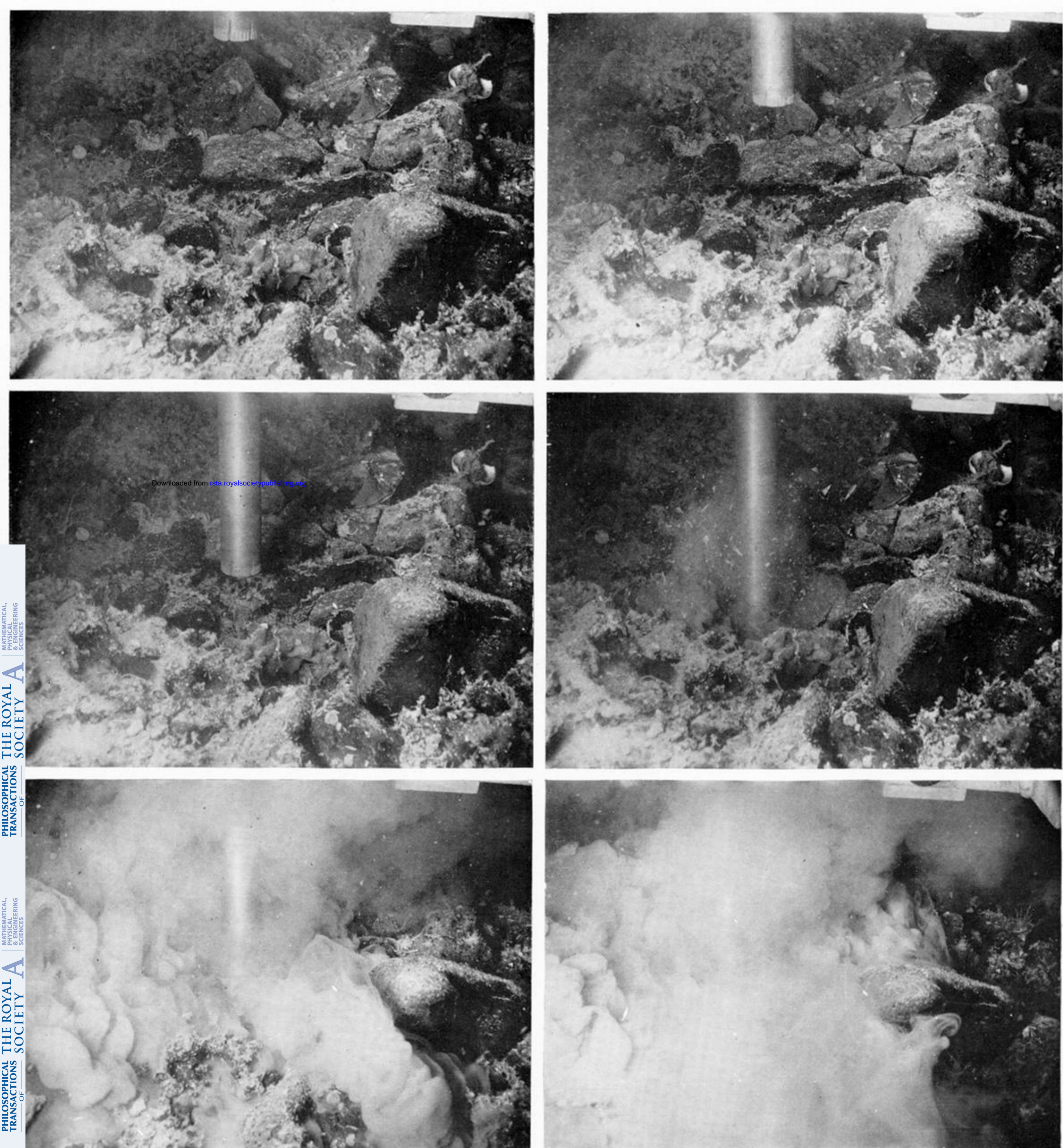
By Y. R. Nayudu

*Institute of Marine Sciences, Douglas, Alaska*

The major physiographic features in the area of investigation include the East Pacific Rise, the Eickelberg Ridge which is a NW trending spur of the East Pacific Rise, and isolated seamounts. Dredge hauls taken between 34 and 3100 m contained fine-grained basalt, porphyritic vesicular basalt, vesicular basalt, glassy basalt, palagonitized glassy basalt, palagonite tuff-breccia, some with manganese encrustations. Most of the rocks are recognizable pillow lava or fragments of pillow basalt. Petro-chemical studies indicate the presence of low potassium tholeiite, alkali basalt and alumina-rich basalt. A discussion on the distribution of trace elements cobalt, nickel, chromium, copper, zinc, rubidium and strontium will be included. A comparative study of these basalts with basalts from the Hawaiian province, basalts of Eocene age from the Oregon Coast Range, basalts from the Mendocino Ridge will be presented.

The present study suggests that high $TiO_2$ and $P_2O_5$ is a distinctive characteristic of alkali basalts and certain related rocks. It is suggested that these parameters ($TiO_2$ and $P_2O_5$) may be as effective an indicator of basalt affinity as the ratio of total alkalis to silica.

The relation of composition of basalt with depth is complex and difficult to judge. Low-potassium tholeiite was dredged from 34 to 2200 m, whereas alkali basalt was from a maximum depth of 2500 m. Vesicle size shows no simple correlation with depth.

K–Ar dating of samples from the area suggests that there was active volcanism during Tertiary time.

Hypotheses concerning the origin of compositional variations will be discussed.

Drilling on the Mid-Atlantic Ridge in 1060 m (F. Aumento, Dalhousie).